General Disclaimer

One or more of the Following Statements may affect this Document

- This document has been reproduced from the best copy furnished by the organizational source. It is being released in the interest of making available as much information as possible.

- This document may contain data, which exceeds the sheet parameters. It was furnished in this condition by the organizational source and is the best copy available.

- This document may contain tone-on-tone or color graphs, charts and/or pictures, which have been reproduced in black and white.

- This document is paginated as submitted by the original source.

- Portions of this document are not fully legible due to the historical nature of some of the material. However, it is the best reproduction available from the original submission.

Produced by the NASA Center for Aerospace Information (CASI)

NSG-1124

(NASA-CR-157228) A FUNDAMENTAL APPROACH TO ADHESION: SYNTHESIS, SURFACE ANALYSIS, THERMODYNAMICS AND MECHANICS Final Report (Virginia Polytechnic Inst. and State Univ.) 143 p HC A07/MF A01 CSCL 07D G3/25

N78-26184

Unclas 16709

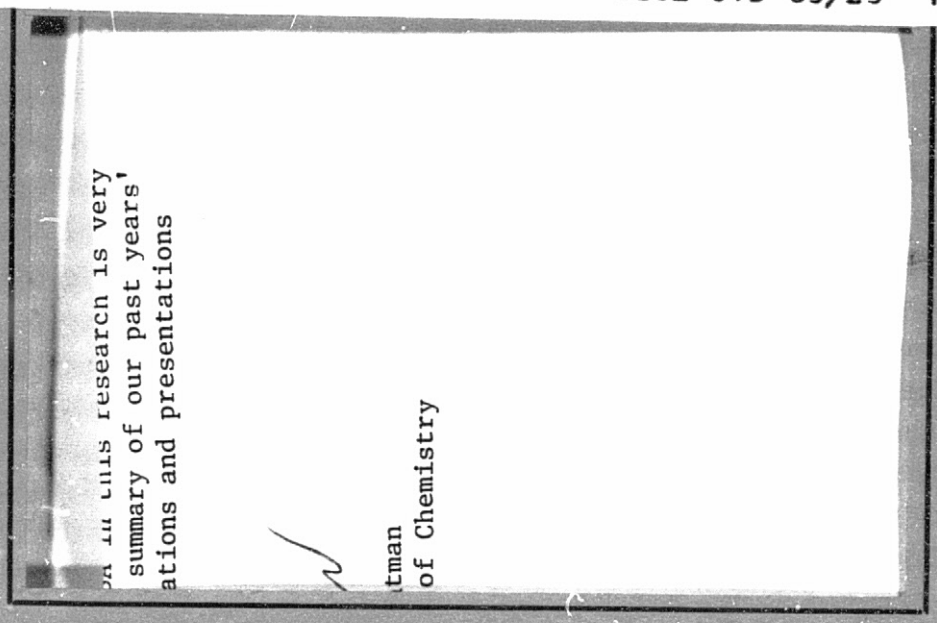

...on of this research is very
...summary of our past years'
...ations and presentations

...tman
of Chemistry

Virginia Polytechnic Institute and State University

Chemistry Department

Blacksburg, Virginia 24061

FINAL REPORT

A FUNDAMENTAL APPROACH TO ADHESION: SYNTHESIS, SURFACE ANALYSIS, THERMODYNAMICS AND MECHANICS

by

Wen Chen, David W. Dwight and James P. Wightman

Prepared for

National Aeronautics and Space Administration

February, 1978

Grant NSG-1124

NASA-Langley Research Center
Hampton, Virginia 23665
Materials Division
Donald J. Progar

Department of Chemistry
Virginia Polytechnic Institute and State University
Blacksburg, Virginia 24061

TABLE OF CONTENTS

LIST OF TABLES

LIST OF FIGURES

GLOSSARY

TECHNIQUES

SEM - Scanning Electron Microscopy

EDAX - Energy Dispersive Analysis of X-ray Fluorescence

ESCA - Electron Spectroscopy for Chemical Analysis (X-ray photoelectron spectroscopy)

ISS - Ion Scattering Spectroscopy

SIMS - Secondary Ion Mass Spectroscopy

AES - Auger Electron Spectroscopy

LEED - Low Energy Electron Diffraction

CHEMICAL, SOLVENTS, ETC.

BTDA - Benzophenone Tetracarboxylic Acid Dianhydride

DABP - Diaminobenzophenone

DG - Diglyme

HT-S - Hercules Graphite fiber

PPQ - Polyphenylquinoxaline

LSS - Lap Shear Strength

Pasa-Jell - Commercial acid etch (See p. 15)

Turco - Commercial base etch (See p. 17)

CTBN - Carboxyl-Terminated Butadiene - acrylonitrile Copolymer

I. INTRODUCTION

This report is the fifth of a series of studies (1,2) on new adhesives, adherends, and interfaces of importance to NASA. Our experimental program mainly employs modern surface analysis techniques to characterize the physical structures and chemical constituents of surfaces before and after bonding and fracture. Table I summarizes the prinicpal areas of effort overall. Two publications submitted during the current grant period are included in the Appendix.

A. Titanium 6-4 Alloy: Surface Treatments and Aging

During the current grant period, primary emphasis has been upon the study of various surface preparations for titanium 6-4 alloy. A new, anodizing method was investigated in particular detail, and compared with the results of other chemical treatments, namely, phosphate/fluoride, Pasa-Jell and Turco. As a first stage in assessing the relative durability of the different surface treatments, changes in surface chemistry and morphology occassioned by aging at 505 K (450^{o}F) were monitored. The scope of the program is outlined in Table II.

Titanium 6-4 alloy, introduced in 1954, is a highly stabilized, alpha-beta phase alloy, using aluminum as the alpha stabilizer and vanadium as the beta stabilizer. These impart toughness and strength at temperatures up to 627 K (750^{o}F). Other alloying elements that favor the alpha crystal structure (hexagonal close pack) at room temperature are gallium, germanium, carbon, oxygen, and nitrogen. The body centered cubic crystal structure, or beta, is stabilized by molybdenum, vanadium, tantalum and columbium. The alloy is protected by an inherent oxide film at low and moderate temperatures, but is subject to oxidation at elevated temperatures. The basic data for applications of titanium and its alloys have been reported (3,4).

TABLE I

SURFACE ANALYSIS AND ADHESIVE BONDING:

EXPERIMENTAL METHODS

I. Scanning Electron Microscopy/Energy Dispersive Analysis of X-rays (SEM/EDAX)

   A. Morphology of Oxide Layers

   B. Identification of Contaminants

   C. Polymer and Composite Fractography

II. Electron Spectroscopy for Chemical Analysis (ESCA)

   A. Oxidation State, Thin Film Composition

   B. Polymer-Surface Structure and Bonding

TABLE II

SURFACE ANALYSIS AND ADHESIVE BONDING. III. TITANIUM 6-4

I. As Received

II. Grit Blast

III. Chemical Treatment and Thermo-oxidative Aging

  A. Anodize

  B. Phosphate/Fluoride

  C. Pasa-Jell

  D. Turco

IV. Analysis of Fractured Lap Shear Specimens

  A. Polyimide and Polyphenylquinoxaline Adhesives

  B. High Temperature Aging and Testing

The general corrosion resistance of titanium and its alloys is superior to many common engineering metals. This is based on a natural, tenacious, self-healing oxide film, usually developed in the environment of water. In the absence of moisture, rapid, pyrophoric oxidation can take place. The oxide film formed in the presence of moisture offers protection at low temperatures, further oxidation of titanium begins to occur at 523 K (480^{o}F).

One of the most important considerations for joining of titanium and its alloys by welding, adhesive bonding, or other techniques is the difficulty of removing contamination. A variety of specialized surface treatments have been developed over the past decade, and increasingly sophisticated measurements are being used to characterize the surfaces involved.

An early report describes the difficulties in working with titanium compared to copper, iron, and aluminum and other metals in common engineering use (5). In a paper which reviewed the application of many techniques of surface analysis to adherends, the use of both alkaline and phosphate/fluoride surface treatments on titanium 6-4 alloy were characterized. Clear differences between treatments were seen by scanning electron microscopy (SEM) and also in surface elemental composition as determined by electron spectroscopy for chemical analysis (ESCA) (6). Moreover, the suggestion was made that the change from anatase to rutile crystal structure made an 8 to 11 percent change in volume, and affected the long term stability of titanium joints. A number of other surface preparations for titanium have been described in the literature (7), including those designed to increase surface hardness by nitriding (8).

More recently there have been a number of publications describing the atomic details of oxidized titanium surfaces. For example, secondary ion

mass spectrometrery (SIMS), Auger electron spectroscopy (AES), and X-ray photoelectron spectroscopy (XPS) (or ESCA) were simultaneously used to study the oxidation of titanium in the monolayer range (9). At high vacuum, oxygen dosages between 133 and 2.66 X 10^3 N m^{-2}sec (1 and 20 Langmuirs) were admitted to a pure titanium surface. The oxygen signals obtained by all three techniques show identical dependence on the oxygen exposure. These data allowed calibration of coverage measurements. Successive stages of oxidation led to significant changes, first in the AES, then in the SIMS signals, and finally to a chemical shift in XPS. An investigation of a number of recommended treatments of titanium 6-4 alloy and pure titanium was undertaken with x-ray and electron diffraction. In this case, no material in the anatase form was found (10).

The oxidation of titanium by water vapor in the 923 to 1223 K range and from 27 to 2400 N m^2 (0.5 to 18 torr) pressure has been recently studied (11). Only one oxide form (rutile) was found and SEM examination of oxidized specimens revealed the presence of whiskers. The pure metal oxidized at a rate about double that of the alloy. Ellipsometry was used to determine the thicknesses of films formed by anodization. Crystal structures were determined by electron diffraction which consisted of either amorphous or the anatase crystal form of TiO_2. The amorphous phase gradually reverted into the rutile structure. An inference was made that this slow, allotropic transformation from anatase to rutile adversely affects the bonding of paint films (12). Low energy election diffraction (LEED) and AES were used to study the reaction of a clean Ti (0001) surface with oxygen at room temperature and dosages between 133 and 1.33 X 10^4 N $m.^{-2}$sec (1 and about 100 Langmuirs). The results indicate that the final film is probably not TiO_2 but rather TiO (13). A different approach to the study of high temperature air oxidation of titanium alloy involved in the use of mass

transport diffusion data in the metallic and oxide phases. A mechanism was determined involving the growth of successive elemental layers. The rate determining step for oxidation was found to be the diffusion of oxygen through a dense elementary layer (14).

An increasing amount of research effort has been spent recently to determine the environmental effects on the failure of structural adhesive joints. The effect of water is a primary concern. In the case of mild steel bonded with epoxy adhesive, the mechanism and kinetics have been identified (15). The nature and topography of fracture surfaces were examined visually and by scanning electron microscopy as well as electron probe microanalysis. Titanium dioxide (5%) in the adhesive was used as a tracer for the electron microprobe. The initial locus-of-failure was found to be primarily cohesive through the adhesive. However, after water immersion, a complex locus-of-failure was found: the path of fracture occurred between the oxide surface layer and the epoxy adhesvie, alternating into the adhesive layer. Cohesive breaking strength of the epoxy resin was determined independently and found to vary differently with temperature than the strength of adhesively bonded joints. It was concluded that the loss in joint strength after immersion in water was the result of the adverse effect of water on the iron surface. In fact, thermodynamic calculations showed that the adhesive layer should be displaced by water. Using the Arrhenius equation, the activation energy for displacement of adhesive by water was determined to be 32 KJ mol^{-1}. This is similar to the value for diffusion of water through an epoxy resin matrix, suggesting that the rate of interface debonding was controlled by the diffusion of water through the adhesive. The corrosion product (Fe_2O_3) was initially absent from the metal fracture surfaces and thus was a post-

failure phenomenon rather than a cuase of failure.

A further set of experiments utilized Auger and x-ray photoelectron spectroscopy to study the locus-of-failure in a similar system (16). The effects of water immersion and silane coupling agents were investigated, and the locus-of-failure determined by microscopy. In dry fractures, the metal resin interface was predominant while water-soaked, unprimed joints fractured interfacially between the adhesive and iron oxide. The application of silane primer prevented formation of an oxide layer and fracture occurred in the silane. The fracture experiments were done within the high vacuum chamber and an ion beam was used to profile through the epoxy or oxide film to more clearly establish the thickness of surface layers.

In a program to determine relative durabilities of adhesive bonded structures, nylon-supported FM400 (a modified epoxy adhesive) was used in conjunction with a corrosion inhibiting primer (17). Six different treatments were applied to the titanium 6-4 alloy and exposure lifetimes determined at 1.03 X 10^7 Nm^{-2} at (1500 psi) stress, 334 K (160^oF) and 100 percent relative humidity. Locus-of-failure was determined visually and samples of lowest life time showed the greatest amount of interfacial failure. Longer-lasting surface treatments (lifetimes varied from 15 to over 1000 hrs.) produced evidence of more cohesive failure in the adhesive layer. The phosphate/fluoride surface treatment showed the lowest lifetime while several other acid treatments (pre-treated with base) produced lifetimes averaging around 500 hrs.

In a study of a proprietary structural adhesive (HT 424) with aluminum 2024-T3 and titanium 6-4, ellipsometry and surface potential difference measurements identified substrates which would result in poor adhesive

bonding (18). The use of Auger spectroscopy with ion-sputtering depth-profiling, electron microscopy and diffraction and x-ray diffraction allowed the locus-of-failure in these systems to be determined. The fracture surface alternated between a surface oxide layer, an interface and primer layer, and into the bulk adhesive. Phosphate/fluoride and Turco surface treatments gave similar bond strength and failure loci. Only a nitric acid/fluoride treatment produced low bond strengths, and this treatment gave large copper concentrations in the oxide film.

Another experimental approach to evaluate different surface treatments determined time-to-failure, or durability, at 333 K ($140^{o}F$) and 95% relativity humidity, at various loads (19). This work indicated the phosphate/fluoride treatment gave stress-durability almost an order of magnitude greater than alkaline-cleaned alloys. Outdoor exposure in both stressed and unstressed adhesive joints indicated a similar comparison between the two surface treatments. Non-destructive thermoholography was able to determine the rearrangement of titanium dioxide under the bond from anatase to rutile crystal structure. Electron diffraction was used to determine the surface structures, which were stabilized with ions that promote anatase (20). To determine the statistical nature of failure under stress in different environments, Weibull distribution parameters were determined from the data (21). A predictive model for failure times of adhesive bonds at constant stress (22) was developed using multiple regression analysis.

In summary, the literature contains useful background information concerning (i) surface analysis of titanium oxidixed with oxygen and water, (ii) Ti 6-4 surface treatment and adhesive bond durability and (iii) epoxy/steel strength, durability and fractography. No publications described Ti 6-4 after anodize, Pasa-Jell or Turco treatments, specifically. Only in

epoxy/steel systems are there correlative data from surface analysis, aging, strength-testing and fractography (15, 16, 18). It is worth mention that these papers are by the recognized authorities in rheology and mechanics, and report the value of modern surface analysis.

Thus we have assurance that our approach is in consonance with the state-of-the-art, and has succeeded in elucidating other structural adhesive bonding problems. Reports do exist on titanium, its alloys and oxides, and adhesive bonding studies. While useful, benchmark comparisons for our experiments can be found, the need is clear for a systematic detailed study of the changes produced in the Ti 6-4 surface during each step of the various preparations, and subsequent thermo-oxidative aging.

B. Adhesive Structure and Bonding, and Fractography

Fundamental studies correlating polymer structure (or more correctly, organic functional groups) with ESCA spectra are needed to firmly establish the technique and provide background information for use of ESCA in practical applications where compositions are unknown. The installation of the DuPont 650 photoelectron spectrometer has greatly facilitated our efforts in this area because spectra are obtained rapidly and displayed directly. This has allowed us to expand the work done last year on the AEI ES-100, and to examine the important, distinctive details such as side-bands and satellite structures.

Spectra have been collected from a wide variety of engineering polymers and copolymers, and also many monomers. Most of the samples do not contain functionality that produce large chemical shifts that facilitate interpretation of ESCA spectra in fluoropolymers or inorganic compounds. Nevertheless, qualitative identification can be effected by careful in-

spection of the peak shapes, positions and intensities, and satellite structures.

Reduction of the ESCA data into publishable form is time-consuming, and still an area of research. For example, deconvolution of overlapping peaks and quantitative ratios of peak areas must eventually become standard procedure. Our spectra from PPQ, LARC-13, and several polyimide monomers needed this data treatment to facilitate interpretation.

The use of a pantograph to reduce the peak sizes so that they can be juxtaposed easily was effective to show some of the potential of ESCA analysis of polymers in cases where distinctive features were clear without deconvolution or quantitative analysis of peak areas. Our initial results in this area have been published (2) and a copy is appended.

SEM/EDAX fractography has been a standard feature of our methods to study failures. During the current grant period, fractured lap shear specimens using PPQ and LARC-13 adhesives were studied, essentially completing a survey of the differences in failure that accompany various combinations of adhesives and adherends.

Short Beam Shear (Interlaminar Shear) testing of fiber-reinforced composite adherends subjects samples to three-point bending to failure. SEM fractography was performed to try to identify the micromechanisms of failure. Similar scouting studies were performed on rubber-toughened epoxy systems. These results will provide a benchmark for future work planned in polyimide toughening.

II. EXPERIMENTAL

A. Apparatus and Procedures

1. Scanning Electron Microscopy/Energy Dispersive Analysis of X-rays (SEM/EDAX)

Photomicrographs were obtained using a Polariod camera back attached to the oscilloscope on the Advanced Metals Research Corporation Model 900 scanning electron microscope. Operating at 20 kV, high magnification views (500X-10,000X) gave information on the details of surface features, while survey scans at 20X-200X provided a check on the distribution of representative features that describe the surface. For convenience in studying the results, approximate vertical dimensions of each photo-micrograph appear at the right in the figures, and the corresponding magnification is listed in each caption. To assist study of some of the photomicrographs, areas seen in higher magnification are indicated by a rectangle drawn on the low-magnification view.

Most specimens were cut to approximately 1 x 1 cm with either a high pressure cutting bar (titanium substrates) or a hack saw (composite substrates), and fastened to SEM mounting stubs with conductive, adhesive-coated, copper tape. A punch-type sample cutter was constructed to obtain 6.4 mm (1/4"), circular samples required for the DuPont 650 ESCA spectrometer, and a few SEM specimens were prepared to determine whether the punch changed surface structures. To enhance conductivity of insulating samples, a thin ($\sim$ 20 nm) film of Au-Pd alloy was vacuum-evaporated onto the samples. Photomicrographs were taken with the sample inclined 70^{o} from the incident electron beam. Rapid, semiquantitative elemental analyses were obtained with an EDAX International Model 707A energy-dispersive X-ray flourescence analyzer attached to the AMR-900 SEM. A Polaroid photographic record of each spectrum was made using a camera specially adapted for the EDAX oscilloscope output.

Tracings of the spectra are juxtaposed in the figures to facilitate interpretation.

2. Electron Spectroscopy for Chemical Analysis (ESCA)

Initially, ESCA data were collected on an AEI ES-100 photoelectron spectrometer using an aluminum anode ($K\alpha_{1,2}$ = 1486.6eV) and digital data acquisition. A Digital PDP-8e computer/plotter was used to deconvolute and display the spectra. Recently we began experiments on a DuPont 650 photoelectron spectrometer with a magnesium anode ($K\alpha_{1,2}$=1253.6eV) and direct display of the spectra on an x-y recorder. This system provided analysis of polymer samples in minutes, a significant advantage for routine work. We are working on more detailed comparisons but the qualitatively distinctive features of polymers are basically the same in both spectrometers.

The carbon 1s level (taken as 284.0 ev for the metal and 285.0 for polymers) evaluate the work function of both spectrometers. Rectangular (5 x 20mm or 100mm^2) samples and circular (6.4mm or 32mm^2) samples were mounted on the sample probes using double sided adhesive tape in the AEI and DuPont spectrometers, respectively. The Ti 6-4 samples were generally cleaned by exposure to a low pressure argon Tesla discharge for 30 seconds.

Wide-scan spectra were obtained to insure that no element present in significant amounts in the surface of the sample is overlooked. The ESCA technique readily detects every element except hydrogen. The DuPont spectrometer is especially suited for rapid analysis; thus, the wide scan ESCA spectra were obtained with the spectrometer. A wide scan (0-700 ev) spectrum can be obtained in about one hour with the DuPont spectrometer. A significantly longer analysis time is required for a similar spectrum to be obtained using the AEI spectrometer. The purpose of obtaining narrow scan spectra was to establish precisely the binding energy, the intensity and the width at half-height of each significant peak noted in the wide scan spectrum.

The elemental assignments of each peak listed in subsequent tables were based on standard binding energy tables (23). A further analysis of the ESCA results are possible using the measured intensities (I_i) in counts/sec listed in Table X and tabulated (24) photoelectric cross sections (σ_i). The following equation approximates the atomic fraction (AF_i) of a given surface species (i):

$$AF_i = \frac{I_i/\sigma_i}{\Sigma\, I_i/\sigma_i}$$

It should be emphasized that such calculations are subject to criticism due to questionable assumptions and at best are only semi-quantitative.

Overlapping or convoluted peaks frequently are obtained, especially in the carbon and oxygen levels where multiple oxidation states are common, but only partially resolved, in specimens of interest to NASA-LaRC. Therefore we have experimented with computer analysis to deconvolute the data into individual components. A transparency of the actual spectra was taped to the front of a Tektronics Graphics Terminal operating on cost sharing in the CMS mode with the University IBM 370 computer. By positioning cursor cross hairs along curves, the spectra were entered digitally. A non-linear regression algorithm then achieved the best fit to a given number of peaks.

B. Materials and Methods

1. Titanium 6-4

An anodized Ti 6-4 sample was obtained from NASA-LaRC and SEM photomicrographs were made on this sample without further treatment. Three additional anodized Ti 6-4 samples (~ 0.5mm thick) were supplied by the Boeing Company. Sample BOE 1 was an anodized specimen. Samples BOE 2 and BOE 3 were opposing members of a fractured peel test specimen in which case, the anodized Ti 6-4 adherends had been bonded with epoxy. Wide scan ESCA spectra for samples

ORIGINAL PAGE IS
OF POOR QUALITY

BOE 1-3 were obtained on the DuPont 650 electron spectrometer. In addition, narrow scan ESCA spectra on samples BOE 1-3 were obtained with the DuPont spectrometer on every significant peak noted in the wide scan spectra. Narrow scan ESCA spectra of carbon, chromium, fluorine, oxygen, and titanium were obtained with the AEI spectrometer on samples BOE 1-3.

Donald Progar, NASA-LaRC Materials Division, supplied "standard" lap shear panels of Ti 6-4, both before and after grit blasting. He also supplied Sprex An-9 alkaline detergent, Pasa-Jell 107 paste and Turco-5578 powder. Three surface treatment processes, listed in Tables III-V, were performed on the Ti 6-4 panels. Samples were taken for analysis by SEM/EDAX and ESCA (DuPont) as described above. Also samples of each of the four surface treatments were exposed for 10 and 100 hours to 505 K (450^{o}F) in an air oven, and subsequently analyzed.

2. Polymers and Composites

Polyimides, and their precursors and polyphenylquinoxalines were supplied by the Polymer Section of the Materials Division at NASA-LaRC. They also formulated the polymers into adhesives, applied them to Ti 6-4 and composites and conducted strength tests. Our ESCA studies were carried out on solvent-cast films or powders. SEM/EDAX results were obtained from the fracture surfaces of lap-shear tested specimens.

Epoxy and two epoxy/CTBN bulk samples were supplied by Goodyear. The formulations are listed in Table VI. Approximately 7.6 x 0.64 x 0.64 cm (3" x 1/4" x 1/4") beams were cut from the samples and fractured in a bending mode. Fracture surfaces were cut off and mounted for SEM.

Cross-sections of composites were obtained by securing samples between rubber faces in a bench-top vice and driving a crack through the sample with one sharp blow of a hammer on hand-held chisel.

TABLE III

PASA-JELL 107 METHOD FOR CLEANING Ti 6-4 PANELS

1. Solvent wipe - methylethyl ketone.
2. Alkaline clean - immerse in SPREX AN-9, 30.1 g/ℓ, 353 K (80^{o}C) for 15 mins.
3. Rinse - deionized water at room temperature.
4. Pickle - immerse for 5 mins at room temperature in solution containing 15g nitric acid (HNO_3) 15% by weight; 3g hydrofluoric (HF) acid 3% by weight; and 82g deionized water.
5. Rinse - deionized water at room temperature.
6. Pasa-Jell 107 Paste: Apply to the titanium surface with an acid resistant brush covering the entire surface by cross brushing.
7. Dry - for 20 mins.
8. Rinse - deionized water at room temperature.
9. Dry - air at room temperature.

TABLE IV

PHOSPHATE/FLUORIDE METHOD FOR CLEANING Ti 6-4 PANELS

1. Solvent wipe - methylethyl ketone.
2. Alkaline clean - immerse in SPREX AN-9, 30.1 g/ℓ, 353 K (80°C) for 15 mins.
3. Rinse - deionized water at room temperature.
4. Pickle - immerse for 2 mins at room temperature in solution containing 350 g/ℓ of 70% nitric acid and 31 g/ℓ 48% HF.
5. Rinse - deionized water at room temperature.
6. Phosphate/fluoride treatment - Soak for 2 mins at room temperature in solution containing 50.3 g/ℓ of tri sodium phosphate (Na_3PO_4); 20.5 g/ℓ of potassium fluoride (KF); and 29.1 g/ℓ of 48% hydrofluoric aicd (HF).
7. Rinse - deionized water at room temperature.
8. Hot water soak - deionized water at 338 K (65°C) for 15 mins.
9. Final rinse - deionized water at room temperature.
10. Dry - air at room temperature.

TABLE V

TURCO 5578 METHOD FOR CLEANING Ti 6-4 PANELS

1. Solvent wipe - methylethyl ketone.
2. Alkaline clean - immerse in Turco 5578, 37.6 g/ℓ, 343-353 K (70-80°C) for 5 mins.
3. Rinse - deionized water at room temperature.
4. Etch - immerse in Turco-5578, 419 g/ℓ, 353-373 K (80-100°C) for 10 mins.
5. Rinse - deionized water at room temperature.
6. Rinse - deionized water at 333-343 K (60-70°C) for 2 mins.
7. Dry - air at room temperature.

TABLE VI

B. F. GOODRICH FORMULATIONS FOR EPOXY AND RUBBER-TOUGHENED RESINS

	C.S. #5606		
	A	B	C
Constituent			
Epon 828 (Shell epoxy)	100	100	100
Bisphenol A	-	-	2
CTBN 1300X8 (Goodrich carboxyl-terminated butadiene-acrylonitrile)	-	5	5
Piperidine	5	5	5

III. RESULTS AND DISCUSSION

A. Titanium 6-4 (SEM/EDAX and ESCA)

This section describes the chemical and physical surface characterization of Ti 6-4 alloy, from manufacture through grit blasting, chemical surface treatment, thermooxidative aging and adhesive bonding. The differences between steps were most apparent in the physical structures that composed the surfaces. Surface chemistry was remarkably constant. Each step will be discussed in turn.

1. As Received.

Scanning electron micrographs of both sides of titanium 6-4 alloy before grit blasting are shown in Fig. 1. The opposing sides are composed of entirely different surface structures. Side A appears to have random, short striations that may be derived from surface working during manufacture or subsequent burnishing or deburring. This side appeared relatively shiny to the eye. Side B, on the other hand, shows no signs of mechanical working, but appears dull to the eye. The difference in surface composition were not entirely removed by chemical treatments such as phosphate/fluoride, and grit blasting was a necessary, intermediate step to produce titanium 6-4 coupon with identical surface structures on both sides. Clearly, the physical differences could cause variations in bond strength values depending upon side.

2. Grit Blasted

After grit blasting the surface appears heavily worked. Fig. 2 shows scanning electron micrographs of a typical example. There is no resemblance of either side to the previous photomicrograph. This surface is composed of deformed and fractured metal and metal oxide. Moreover, it is covered with fracture debris in the size range 0.1 to 10 μm. None of the particles on

FIGURE 1

Two magnifications (200X, 10,000X) of both sides of a Ti 6-4 coupon before grit blasting.

FIGURE 1. Two magnifications (2000X, 10,000X) of both sides of a Ti 6-4 coupon before grit blasting.

Side A is shiny to the eye and at 2000X striations that appeared to be caused by metal working occur that do not show on Side B. Clearly the two sides have entirely different physical structures that may produce different results in adhesion.

ORIGINAL PAGE IS
OF POOR QUALITY

FIGURE 2

Four magnifications (500X, 2000X, 5000X, 10,000X) of a grit blasted sample of Ti 6-4.

FIGURE 2. Four magnifications (500X, 2000X, 5000X, 10,000X) of a grit blasted sample of Ti 6-4.

This appears to be the heavily worked, fragmented remains of the previous Ti 6-4 sample. Fracture debris, 0.1 μm <d<10 μm, are densely scattered. Excess aluminum content was shown by EDAX (Figure 3).

ORIGINAL PAGE IS
OF POOR QUALITY

this substrate resembles grit blast particles (2). However, the aluminum content of this surface was shown by energy dispersive x-ray analysis (EDAX) to be unusually high. Fig. 3 compares the EDAX results from Ti 6-4 after grit blast, and subsequent phosphate/fluoride etch, and a grit blast particle. The aluminum content of the grit blasted sample is about an order of magnitude greater than titanium 6-4 alloy. Also the Al was uniformly distributed over the surface; the fracture debris particles showed the same EDAX spectrum as the substrate. In Fig. 3 the results from alumina grit blast particle shows a much greater ratio of aluminum to titanium. The ESCA results from these samples, shown in Tables VII-A and VII-B, confirm that the grit blasted sample has the highest aluminum content. Also, the carbon content is highest indicating organic contamination, not unexpected in a grit blast operation. The ESCA results obtained after thermo-oxidative aging are shown in Table VIII.

3. Chemical Treatment and Thermo-oxidative aging

a. Anodize. The anodized specimen with a proprietary (Boeing Company) surface treatment was obtained from NASA-LaRC. Scanning electron micrographs before and after thermo-oxidative aging for ten hours at 505 K (450^{o}F) are shown in Fig. 4. There appears to be a very thin oxide layer on the surface with minute cracks or fissures of irregular shape, densely populating the surface. These cracks have sharp edges at the upper surface and where they meet the underlaying substrate. At highest magnification the whole surface appears to be sponge-like with fine pores of diameter < 5 μm. After aging some connecting of the irregular cracks in the surface oxide layer appears to occur. However, at high magnification it appears that the oxide layer is more firmly adherent to the underlaying substrate.

The ESCA results listed in Tables IX and X for the three samples obtained from the Boeing Company are discussed below by element.

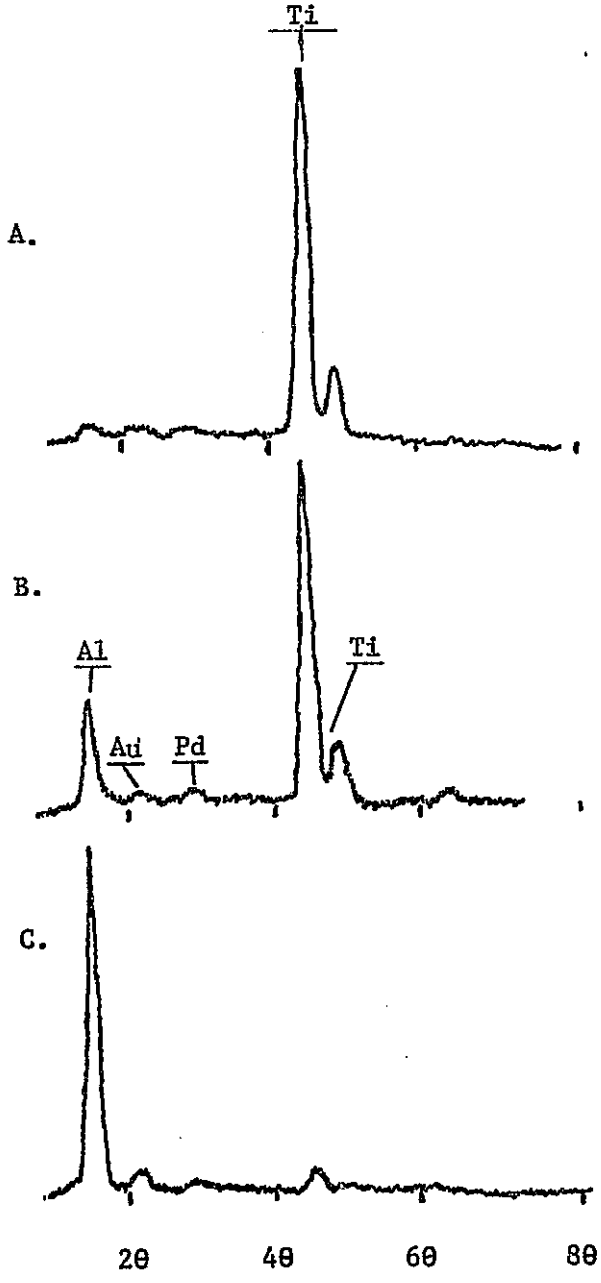

ORIGINAL PAGE IS
OF POOR QUALITY

Figure 3. EDAX Spectrum typical of Ti 6-4 Coupon.

A. After surface treatments.

B. After grit blast.

C. Particles found on samples received 10/76.

TABLE VII-A

ELEMENTAL ASSIGNMENTS AND PEAK PARAMETERS
FOR Ti 6-4 GRIT BLASTED SAMPLES AFTER CHEMICAL TREATMENT

Element	GRIT BLAST			PASA-JELL I			PASA-JELL II		
	BE	I	W	BE	I	W	BE	I	W
Ti 2s		NS		564.6	1.0	6.0	564.5	1.0	4.2
Ti $2p_{1/2}$	463.7	2.0	2.2	463.6	3.0	2.2	463.4	5.6	2.2
Ti $2p_{3/2}$	457.9	5.0	1.6	457.7	10.0	1.6	457.5	13.1	1.4
Ti 3s		NS		61.3	< 1.0	2.8		NS	
Ti $3p_{1/2}$		NS		36.2	1.0	2.2	35.5	2.0	2.0
O 1s	530.0	21.0	1.8	529.4	41.0	2.0	529.7	38.0	2.0
C 1s	284.0	53.0	1.8	284.0	30.0	1.6	284.0	35.5	1.8
F 1s	684.2	2.0	3.5	684.1	2.0	2.2	685.3	<1.0	2.0
F (A)		NS		595.4	-	7.0		NS	
Cr $2p_{1/2}$		-		586.0	<1.0	2.6	586.1	<1.0	2.0
Cr $2p_{3/2}$		-		576.4	2.0	3.2	576.2	2.0	3.6
Cr 3s		-			-			-	
Si 2s		-		154.3	2.0	2.8	153.4	1.0	3.0
Si 2p		-		103.2	3.0	2.0	103.4	<1.0	3.0
Al 2s	118.5	8.0	2.6	119.2	2.0	2.8	116.9	1.0	4.0
Al $2p_{1/2}$	73.6	9.0	2.2	73.4	<1.0	2.3	73.5	<1.0	3.0
V $2p_{3/2}$	514.2	<1.0	2.0	514.6	<1.0	1.8		NS	
Na A		-			-			-	
Zn A		-			-			-	
Cl $2p_{1/2}$		-			-			-	

TABLE VII-A (Continued)

Element	GRIT BLAST BE	GRIT BLAST I	GRIT BLAST W	PASA-JELL I BE	PASA-JELL I I	PASA-JELL I W	PASA-JELL II BE	PASA-JELL II I	PASA-JELL II W
P $2p_{3/2}$		-			-			-	
Ca $2p_{1/2}$	350.4	<1	2.2		-			-	
Ca $2p_{3/2}$	346.6	<1	2.4		-			-	
N 1s		-			-			-	
K $2p_{1/2}$		-			-			-	

BE = corrected binding energy (ev), C_{1s} as internal standard.

I = relative intensity (corrected by cross section)

W = peak width at half height.

NS = Not scanned

- = no significant peak

TABLE VII-B
ELEMENTAL ASSIGNMENTS AND PEAK PARAMETERS
FOR Ti 6-4 GRIT BLASTED SAMPLES AFTER CHEMICAL TREATMENT

Element	TURCO (I)			TURCO (II)			PHOSPHATE-FLUORIDE (I)			PHOSPHATE-FLUORIDE (II)		
	BE	I	W	BE	I	W	BE	I	W	BE	I	W
Ti 2s	564.5	1.0	5.4	564.3	1.0	4.2	564.6	1.0	5.2	564.4	1.4	4.6
Ti $2p_{1/2}$	463.8	3.0	2.2	463.0	3.0	2.2	463.7	4.0	2.2	463.6	5.0	2.4
Ti $2p_{3/2}$	458.0	9.0	1.6	457.7	10.0	1.4	457.9	15.0	1.5	456.1	14.8	1.8
Ti 3s		-			-			-		61.2	<1.0	2.8
Ti $3p_{1/2}$		-			-			-		36.2	2.0	2.2
O 1s	529.4	32.0	2.0	529.4	29.0	2.0	529.4	38.0	2.0	529.6	39.4	2.0
C 1s	284.0	52.0	1.6	284.0	47.0	1.6	284.0	38.0	1.6	284.0	27.2	2.0
F 1s		NS		685.0	5.0	3.7	684.4	<1.0	2.0	684.0	3.8	2.6
F A		-			-			-			-	
Cr $2p_{1/2}$		-			-			-			-	
Cr $2p_{3/2}$		-			-			-			-	
Cr 3s		-			-			-			-	
Si 2s		-			-			-			-	
Si 2p		-			-			-			-	
Al 2s	119.1	1.0	3.2		NS		118.2	1.0	2.0		NS	
Al $2p_{1/2}$	73.6	2.0	2.2		NS		73.4	1.0	2.0		NS	
V $2p_{3/2}$	515.3	<1.0	2.2	516.0	1.0	1.4	515.3	<1.0	2.4	515.6	<1.0	2.0
Na A		-			-			-			-	
Zn A		-			-			-			-	

TABLE VII-B (Continued)

Element	TURCO (I) BE	TURCO (I) I	TURCO (I) W	TURCO (II) BE	TURCO (II) I	TURCO (II) W	PHOSPHATE-FLUORIDE (I) BE	PHOSPHATE-FLUORIDE (I) I	PHOSPHATE-FLUORIDE (I) W	PHOSPHATE-FLUORIDE (II) BE	PHOSPHATE-FLUORIDE (II) I	PHOSPHATE-FLUORIDE (II) W
Cl $2p_{1/2}$		-			-			-		197.3	1.0	3.8
P $2p_{3/2}$		-			-			-		132.6	1.0	2.0
Ca $2p_{1/2}$		-			-			-			-	
Ca $2p_{3/2}$		-			-			-			-	
N 1s		-			-			-			-	
K $2p_{1/2}$		-			-			-		287.9	2.0	1.6

TABLE VIII

ELEMENTAL ASSIGNMENTS AND PEAK PARAMETERS
FOR Ti 6-4 GRIT BLASTED SAMPLES AFTER CHEMICAL TREATMENTS AND THERMO-OXIDATIVE AGING
IN AIR AT 505 K (450°F), FOR 10 HOURS

Element	PASA-JELL			TURCO			PHOSPHATE/FLUORIDE		
	BE	I	W	BE	I	W	BE	I	W
Ti 2s	564.1	1.0	5.6	564.4	1.0	4.8	564.4	1.2	4.6
Ti $2p_{1/2}$	463.1	4.1	2.4	463.4	6.0	2.4	463.6	5.1	2.4
Ti $2p_{3/2}$	457.3	12.5	1.6	457.5	13.0	1.6	457.8	14.1	1.6
Ti 3s	60.9	<1.0	2.6	61.3	<1.0	2.8	61.4	<1.0	2.6
Ti $3p_{1/2}$	35.9	1.2	2.2	36.0	1.0	2.4	36.2	1.5	2.4
O 1s	529.1	33.0	2.0	529.4	41.4	2.0	530.2	32.1	2.0
C 1s	284.0	43.4	1.6	284.0	33.1	1.8	284.0	42.5	1.7
F 1s		-			-			-	
F A		-			-			-	
Cr $2p_{1/2}$	585.9	<1.0	3.4		-			-	
Cr $2p_{3/2}$	576.5	<1.0	3.6		-			-	
Cr 3s		-			-			-	
Si 2s	154.1	<1.0	3.0		-			-	
Si 2p	103.1	<1.0	2.6		-			-	
Al 2s	117.7	1.0	2.0	117.8	1.0	2.0		NS	
Al $2p_{1/2}$	73.1	1.3	2.0		-			-	
V $2p_{3/2}$	515.7	<1.0	1.6	516.8	1.0	2.0		NS	
Na A		-			-			-	

TABLE VIII (Continued)

Element	PASA-JELL BE	PASA-JELL I	PASA-JELL W	TURCO BE	TURCO I	TURCO W	PHOSPHATE/FLUORIDE BE	PHOSPHATE/FLUORIDE I	PHOSPHATE/FLUORIDE W
Zn A		-			-			-	
Cl $2p_{1/2}$		-			-			-	
P $2p_{3/2}$		-			-		132.4	1.5	2.0
Ca $2p_{1/2}$		-			-			-	
Ca $2p_{3/2}$		-			-			-	
N 1s	398.9	<1.0	2.0	398.8	<1.0	3.2	398.8	1.0	2.4
K $2p_{1/2}$		-				-		-	

FIGURE 4

Two magnifications (2000X, 10,000X) of Ti 6-4 surface after anodizing.

FIGURE 4. Two magnifications (200X, 10,000X) of Ti 6-4 surface after anodizing. A. Before and B. After exposure to air at 505 K (450°F) for 10 hours.

An entirely unique surface morphology appears after anodizing. There appears to be a thin surface oxide layer permeated with many microfissures of irregular dimension. Moreover, at high magnification fine microporosity appears as a uniform constituent of the oxide surface. Some change does occur in Side B after thermo-oxidative aging, but it appears less than in the acidic and basic chemical treatments (Figs. 2-7). After aging the fissures seem to elongate or broaden and show a greater level of connectiveness. Also, the oxide layer appears thinner, or more firmly adherent to the underlying substrate.

A

50 μm

10 μm

B

50 μm

10 μm

ORIGINAL PAGE IS
OF POOR QUALITY

TABLE IX

ELEMENTAL ASSIGNMENTS AND PEAK PARAMETERS
FOR Ti 6-4 ANODIZED SAMPLES

	BOE 1			BOE 2			BOE 3		
Element	BE	I	W	BE	I	W	BE	I	W
F 1s	684.1	1840	2.2	684.6	640	3.0	684.7	3080	2.4
F(A)		NS*			NSP**			NS	
F(A)	596.0	920	4.2	595.0	400	7.4	596.2	1460	4.8
Ti 2s	564.6	1100	7.0	564.3	1420	4.2	565.2	1020	6.2
O 1s	529.9	13800	2.8	529.5	28800	2.0	530.0	14700	2.0
V $2p_{3/2}$	515.0	310	2.6	514.9	180	3.2		NSP	
Ti(IV) $2p_{1/2}$	463.7	4100	2.1	463.7	5000	2.4	464.4	3300	2.4
Ti(IV) $2p_{3/2}$	457.9	13100	1.6	457.9	17300	1.6	458.6	11400	2.0
Ti(O) $2p_{3/2}$		NSP		453.0	800	1.6		NSP	
Ti(IV) $2p_{3/2}(K\alpha_{3,4})$	449.1			449.6				NS	
N 1s	399.2	400	2.2	399.3	540	2.4	399.6	500	3.0
C 1s	(284.0)	28000	1.6	(284.0)	28000	1.6	(284.0)	21800	1.6
C 1s $(K\alpha_{3,4})$	275.0	2000	3.2		NS		275.4	1800	3.4
Cl 2p	197.6	240	2.4	198.3	180	5.0		NSP	
Al 2s	118.2	240	2.6	118.1	380	3.0	119.0	300	3.0
Al 2p	72.6	400	3.2	73.4	440	2.4	74.2	320	2.2
Ti 3s	60.8	640	3.0	61.3	660	4.0	61.8	560	3.2
	50.0	220	6.0	50.3	200	5.0	[52]***		
Ti(IV) 3p	35.8	1620	2.6	36.3	1880	2.8	36.9	1520	3.6
Ti(O) 3p		NSP		31.3	200	1.0		NSP	
Cr		NSP			NSP			NSP	
ϕ (ev)	3.0			0.7			1.6		

*NS - not scanned
**NSP - scanned but no significant peak observed
***Values appearing in brackets were read directly off of wide scan spectra and so are less precise than unbracketed values read directly off of narrow scan spectra.

TABLE X

ATOMIC COMPOSITION OF ANODIZED Ti 6-4 SAMPLES

Element	Photoelectric Cross-section	Atom Percent		
		BOE 1	BOE 2	BOE 3
F 1s	4.26	1.2	0.4	2.4
O 1s	2.85	13.2	23.6	16.9
V $2p_{3/2}$	6.33	0.1	0.1	NSP*
Ti(IV) $2p_{3/2}$	5.22	6.9	7.8	7.1
Ti(O) $2p_{3/2}$	5.22	NSP	0.4	NSP
N 1s	1.78	0.6	0.7	0.9
C 1s	1.00	76.6	65.5	71.3
Cl $2p_{3/2}$	1.56	0.4	0.3	NSP
Al $2s_{1/2}$	0.681	1.0	1.3	1.4

*NSP - no significant peak

Fluorine. Fluorine, presumably present as a fluoride species, was detected in all samples. Fluorine gives an Auger peak at 595.6 ± 0.6 ev in addition to the 1s photopeak at 684.4 ± 0.3 ev.

Oxygen. Intense oxygen 1s photopeaks (529.6 ± 0.4 ev) were observed for each sample. Since an oxide layer would be expected to be present in each case, this result is not too surprising. It might be expected that the O/Ti ratio would be 2:1. However, this ratio varies from 1.9:1(BOE 1) to 3.0:1(BOE2). The excess oxygen may be due to the certain presence of adsorbed water in the oxide films not removed by low temperatures outgassing in the spectrometer.

Vanadium. Since vanadium is one of the components of the Ti 6-4 alloy, its presence is again not surprising. However, its surface concentration is constant and extremely small at about 0.1%. The stoichiometric ratio of Al/V should be 1.5. The fact that the value of the ratio is higher bespeaks the considerable enhancement of aluminum at the surface of the alloy.

Titanium. Interesting results were obtained for this major element in that elemental titanium [Ti (0)] was observed in sample BOE 2. Titanium combined in the tetravalent state [Ti (IV)] presumably as the oxide was observed in all three samples. The major titanium oxide $2p_{1/2}$ and $2p_{3/2}$ photopeaks were observed at 464.0 ± 0.2 and 458.2 ± 0.2 ev, respectively. The separation of the two peaks by 5.8 ± 0.4 ev is in excellent agreement with the published separation of 6 ev (23, 24). The elemental titanium $2p_{3/2}$ photopeak appeared at 452.8 ± 0.2 ev, 5.4 ev lower than the titanium present as an oxide. Supporting evidence for this assignment is in the titanium 3p photopeak at 36.4 ev. Again, in sample BOE 2, a smaller peak was observed at 31.2 ± 0.1 ev. The separation of 5.2 ev compared to 5.4 ev above supports the conclusion that the lower binding energy peak is due to elemental titanium. The fact the elemental titanium is observed at all indicates an ultra-thin oxide layer (< 100 A) in the case of BOE 2. Thicker oxide layers must be present in the other samples since no elemental titanium signal was observed. It should be remembered that none of the samples were given any special pretreatment such as ion etching. Thus, it is possible to have a thin oxide film on Ti 6-4 after exposure to air for an extended period of time at ambient temperature. In the case of BOE 2, the amount of elemental titanium is some twenty times less than that present as oxide.

Smaller 2s and 3s photopeaks of Ti are noted at 564.7 ± 0.3 and 61.4 ± 0.2 ev, respectively. Finally, since a monochromatic Mg x-ray source was not used, less intense (by at lest a factor of ten) photopeaks ($K\alpha_{3,4}$) should appear about 9.3 ev lower than the intense photopeak ($K\alpha_{1,2}$). In fact, the $K\alpha_{3,4}$ $2p_{3/2}$ photopeak for Ti (IV) appeared 8.6 ± 0.1 ev below the $K\alpha_{1,2}$ peak.

Nitrogen. A fairly constant small nitrogen content (0.7 ± 0.1%) was noted in all samples. The 1s photopeak at 399.4 ± 0.2 ev is in excellent agreement with the value of 399.3 ± 0.2 ev reported earlier by Bush, Counts and Wightman (25).

Carbon. The high carbon content (50-77%) in the surface of all samples may at first be surprising. However, the ESCA technique only detects elements in the surface layer (< 10 nm). Organic contamination invariably gives rise to a large carbon 1s photopeak and in the present work a less intense $K\alpha_{3,4}$ 1s photopeak 8.8 ± 0.2 ev lower than the $K\alpha_{1,2}$ peak. Since no attempt was made to pretreat the samples prior to ESCA analysis, a predominant carbon signal is generally observed. Recent work in our laboratory has shown for example that the carbon signal on iron foil can be reduced by a factor of 2 by a 60 second exposure to an Ar glow discharge.

Chlorine. Chlorine, presumably present as chloride ion, was detected in some samples by a very weak 2p photopeak at 197.9 ± 0.3 ev. The origin of the chloride is not clear.

Chromium. Although chromium was shown by the AEI spectrometer to be present at small levels in the samples, no significant Cr signal was noted in any of the samples using the DuPont spectrometer. Scans for Cr were made over the range 575 to 590 ev corresponding to the most intense photopeaks.

A small peak was observed in all samples at 50.4 ± 0.2 ev, but no definitive elemental assignment was made.

Summarily, it should be re-emphasized that the calculated surface compositions are only semi-quantitative at best. Care should be exercised in interpreting these results. On the other hand, the ESCA technique has

given nearly unique information about the samples. Most analytical techniques result in bulk elemental analyses. The ESCA technique has given elemental analysis about the surface layer (< 10 nm) only. The relation of the ESCA techniques to adhesion is direct. Indeed, it is in this interfacial region (< 10 nm) where attention is focused in many adhesive systems.

Since ESCA data was collected on both the AEI and DuPont spectrometers, it is of interest to compare the results. A tabulation of binding energies, intensities and width at half-height for Ti, Cr, F, O and C obtained from both spectrometers on samples BOE 1-3 is given in Table XI.

The first point to note is the following remarkable consistency in the binding energies (BE):

Element	AEI	DuPont
F	684.4 $\pm$ 0.1	684.5 $\pm$ 0.2
O	529.7 $\pm$ 0.2	529.8 $\pm$ 0.2
Ti $2p_{3/2}$	458.0 $\pm$ 0.3	458.1 $\pm$ 0.3

The peak shapes are similar as gauged by a comparison of the peak widths at half-height (W). Neither spectrometer gives consistently narrower peaks. A significantly broader O 1s peak in Sample BOE 1 was noted in the DuPont spectrometer. Comparison of oxygen 1s - DuPont with oxygen 1s - AEI shows that both peaks appear to be a composite of at least two peaks. That is, both peaks are asymmetric due to a shoulder on the high energy size. The larger peak width in the case of the DuPont data is caused by a more intense high energy component. Thus, oxygen is bound in at least two modes in the Ti 6-4 samples. The smaller, lower binding energy peak due to elemental titanium was clearly seen in the narrow scan spectrum from both the AEI and the DuPont spectrometers.

TABLE XI

COMPARISON OF AEI AND DUPONT SPECTROMETERS FOR Ti 6-4 ANALYSIS

	BOE 1						BOE 3					
	AEI			duPont			AEI			duPont		
Element	BE	I	W	BE	I	W	BE	I	W	BE	I	W
F 1s	684.2	62	2.0	684.1	1840	2.2	684.5	332	2.2	684.7	3080	2.4
Cr	577.2	12	6.0				577.4	12	7.5			
O 1s	529.9	694	2.0	529.9	13800	2.8	529.8	413	2.2	530.0	14700	2.0
Ti(IV) $2p_{1/2}$	464.0	170	2.5	463.7	4100	2.1	463.5	118	2.7	464.4	3300	2.4
Ti(IV) $2p_{3/2}$	458.3	546	1.6	457.9	13100	1.6	458.2	345	2.0	458.6	11400	2.0
Ti(O) $2p_{3/2}$												
C 1s	(284.0)	324	1.5	(284.0)	28000	1.6	(284.0)	205	1.8	(284.0)	21800	1.6

	BOE 2					
	AEI			duPont		
Element	BE	I	W	BE	I	W
F 1s	684.4	28	2.6	684.6	640	3.0
Cr	578.6	16	11.1			
O 1s	529.4	820	1.9	529.5	28800	2.0
Ti(IV) $2p_{1/2}$	463.1	145	2.3	463.7	5000	2.4
Ti(IV) $2p_{3/2}$	457.6	514	1.7	457.9	17300	1.6
Ti(O) $2p_{3/2}$	452.5	80	1.7	453.0	800	1.6
C 1s	(284.0)	255	1.8	(284.0)	28000	1.6

Cr was detected in the AEI spectrometer but not in the DuPont spectrometer. In this case where the chromium concentration is $\sim$ 0.3% (on the same scale in Table X), the repetitive scan capability of the AEI is superior to the analog mode of the DuPont. Parenthetically, the DuPont also has repetitive scan capability which was not used in this work. In physical terms, for Cr analysis, the DuPont is detecting a small change in electron intensity in a binding energy region where a large number of background electrons are being collected.

The final point is the significant difference in intensities (I) obtained with the two spectrometers. Since the DuPont spectrometer was run in the analog mode in all cases, the intensities were calculated directly from the narrow scan spectra by the relation $I = PH \times S$. Here PH is the measured peak height (in cm) and S is the selected sensitivity (in counts/sec/cm).

The AEI spectrometer is computer interfaced and the ESCA spectra obtained result from multiple scans. In order to compare intensities between the two spectrometers, the relation $I = PH \times \Delta/(FSH \times T \times NS)$ was used for the AEI data. Here Δ is the difference between maximum and minimum counts (an output parameter), FSH is the full scale height (in cm - the ordinate height in the plotted spectrum), T is the time per channel (in sec - an output parameter) and NS is the number of scans (an output parameter).

The intensities obtained with the DuPont are typically some 30 times greater than those obtained with the AEI. The AEI uses a slit between the sample and analyzer so that only a fraction of the total photoejected electrons are analyzed. In contrast, the DuPont spectrometer collects and analyzes most of the photoejected electrons. So the large differences in

intensity for the two spectrometers is not unexpected.

In summary, for the analysis and anodized Ti 6-4 samples, the binding energies obtained with the two spectrometers were in excellent agreement. There was no consistent trend in peak widths between the two spectrometers. This difference in intensity results in a faster analysis in the DuPont spectrometer. For example, actual analysis time for the five elements in BOE 1 was 33 minutes for the DuPont spectrometer and 210 minutes for the AEI spectrometer.

b. Phosphate/Fluoride. Scanning electron micrographs of phosphate/fluoride-etched Ti 6-4 before and after aging are shown in Fig. 5. Before aging (A) there appears fairly well defined gray alpha and white beta phases. At high magnification the beta phase crystals are poorly defined, but the alpha phase shows regularly-spaced edges approximately 100 nm units apart. After aging the surface becomes covered with a dense packing of small nodules approximately 100 nm in diameter. Both alpha and beta phase are still distinguishable, however it appears that the alpha phase has grown at the expense of the beta during oxidation. The ESCA results shown in Table VII-B indicate a trace of phosphorous and fluorine adsorbed during the surface treatment process and retained in the surface through the rinsing step. Otherwise the ESCA spectra are quite similar to Pasa-Jell and Turco results.

c. Pasa-Jell. Fig. 6 shows scanning electron micrographs of the Ti 6-4 surface after Pasa-Jell treatment and thermo-oxidative aging. The beta phase is larger than in the previous case and more clearly defined in white, plate-like crystallites. On the other hand, the gray, alpha phase shows less distinct crystalline development. An artifact appears in these photo-

FIGURE 5

Two magnifications (2000X, 10,000X) of Ti 6-4 surface after phosphate/fluoride treatment.

FIGURE 5. Two magnifications (2000X, 10,000X) of Ti 6-4 surface after Phosphate/Fluoride treatment.

A. Before and B. After exposure at 505 K (450°F) for 10 hrs. in air.

Well defined originally, there is a gray alpha phase and a discontinuous, white beta phase. After aging similar overall features remain but are less sharp; edges appear to be rounded. At high magnification, the surface appears to consist of the dense packing of very small modules.

ORIGINAL PAGE IS
OF POOR QUALITY

A

50 μm

10 μm

B

50 μm

10 μm

ORIGINAL PAGE IS
OF POOR QUALITY

FIGURE 6

Two magnifications (2000X, 10,000X) of Ti 6-4 surface after Pasa-Jell process.

FIGURE 6. Two magnifications (2000X, 10,000X) of Ti 6-4 surface after Pasa-Jell process. A. Before and B. After aging in air at 505 K (450°F) for 10 hours.

Note that the white, beta phase particles are larger and more crystal-like than in the previous sample. The small white "popcorn" particles appear to be artifacts of the last step of process (See Fig. 6). After aging (Side B), nodules do not appear as in the previous case, but the sharpness decreased and the beta phase particles diminish in size and number, appearing to submerge into the surface.

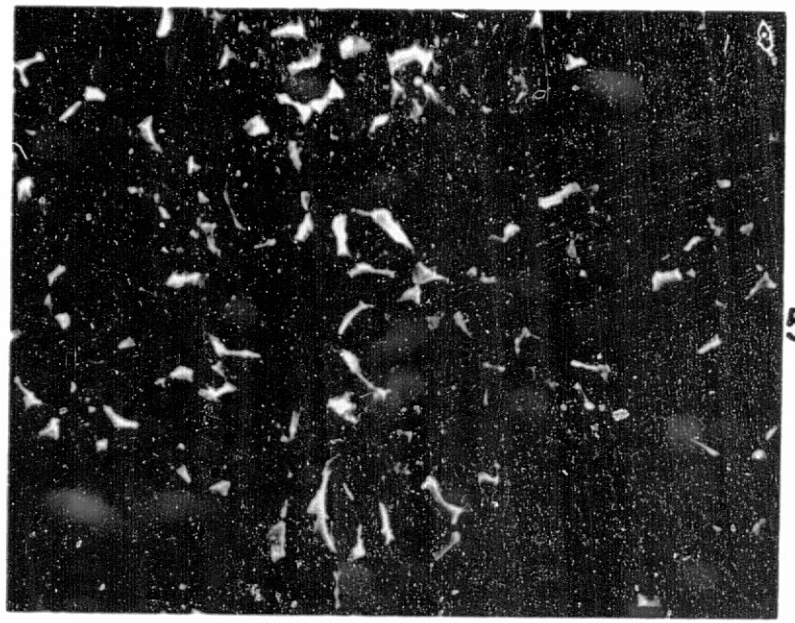

A

50 μm

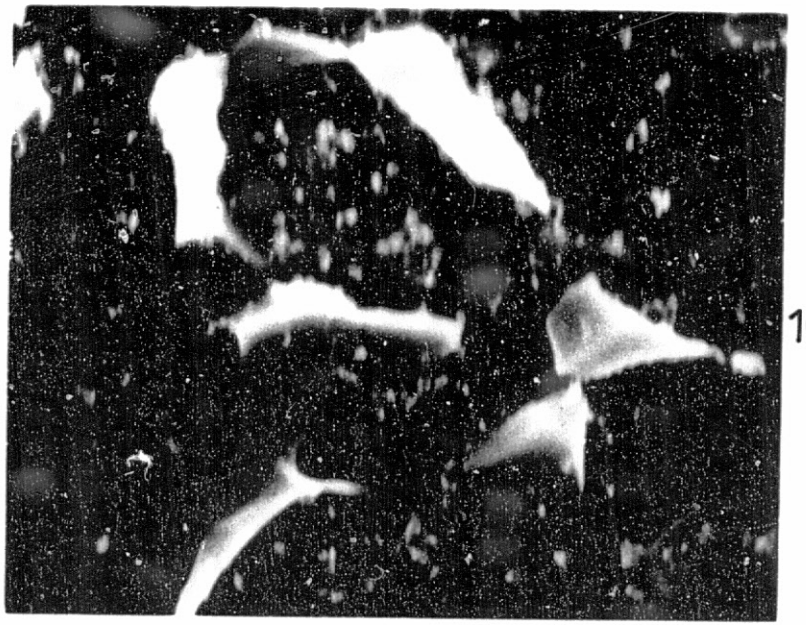

10 μm

ORIGINAL PAGE IS
OF POOR QUALITY

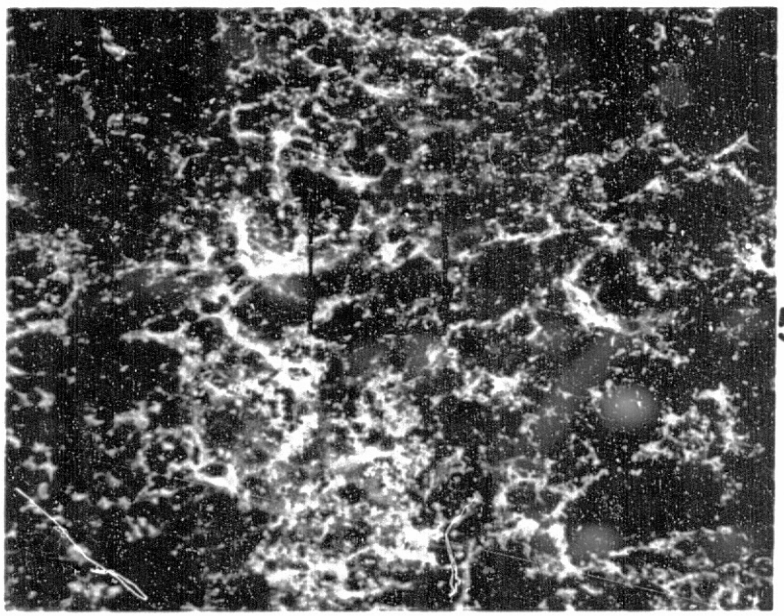

B

50 μm

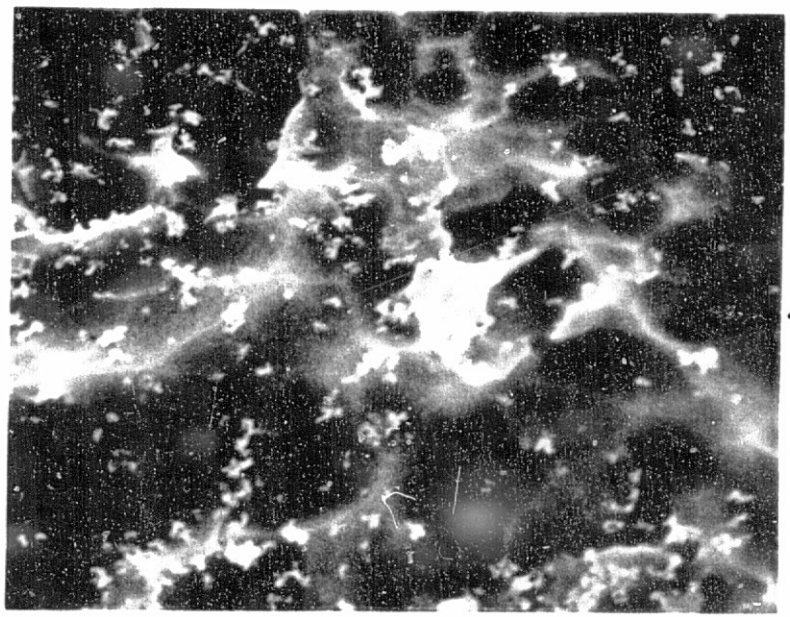

10 μm

micrographs in the form of "popcorn" particles approximately 50 nm in diameter. (These are shown to occur in step 6 of the Pasa-Jell process (see Table III) as noted in comparing Figures 6 and 7. After aging the beta phase appears to have diminished dramatically. Those few beta phase particles that still appear seem to have been absorbed into the surrounding alpha-phase matrix. The ESCA results in Table VII-A show higher aluminum content in the case of the Pasa-Jell process than in either of the other chemical surface treatments. Moreover, chromium and silicon are exclusive surface components after Pasa-Jell treatment. The presence of these elements is not unexpected since compounds containing these elements are in the Pasa-Jell 107 paste.

Figure 7 shows the titanium 6-4 alloy after all but the final application of the acid-jell in the Pasa-Jell process. Clearly the surface shows less developed alpha and beta phase and appears to consist more of amorphorous oxide in greater thickness. However, the "popcorn" particles do not appear, and thus we conclude that they were artifacts carried on the the surface by the specific lot of the Pasa-Jell paste.

Both phosphate/fluoride and Pasa-Jell treatments are acidic, and they result in surface structures that are similar.

d. Turco. The Turco process exposed Ti 6-4 alloy to basic solutions. Scanning electron micrographs of the results are shown in Fig. 8. This surface is entirely different from any of the previous surface treatments morphologies. There is no clear distinction between alpha and beta phase, which leads to the impression that the surface is a pure oxide layer without separate alloy phases. The oxide layer is well defined and high fragmented at the asperities on the surface. The results of thermo-oxidative aging are more dramatic in the case of Turco surface treatments than in the previous cases. Shown in Side B of Figure 8, it appears that the surface

FIGURE 7

Two magnifications (2000X, 10,000X) of Ti 6-4 surface after Pasa-Jell process except final step.

FIGURE 7. Two magnifications (2000X, 10,000X) of Ti 6-4 surface after the Pasa-Jell process except step 6.

The clear alpha/beta phase sturcture has not materialized but the "popcorn" particles are no longer present, indicating they arise during step 6 of the Pasa-Jell treatment.

ORIGINAL PAGE IS
OF POOR QUALITY

FIGURE 8

Two photomicrographs (2000X, 10,000X) of Ti 6-4 surface after Turco process.

ORIGINAL PAGE IS
OF POOR QUALITY

FIGURE 8. Two photo-micrographs (2000X, 10,000X) of Ti 6-4 after Turco process. A. Before and B. After exposure to air at 505 K (450°F) for 10 hours.

The surface structures are very different from the preceeding two acid treatments. The difference in phases is not clear and it appears that surface consists of a fragmented oxide layer. In B., profound rearrangement of the surface topography has occured during heating. There appears to be an attempt on the part of the surface structure to align in a plate-like configuration. This alignment seems to produce more fracture surface features. At highest magnification there appears a fine texture on the surfaces that was absent before heating.

topography has collapsed to some degree into locally-ordered plane- or plate-like structures that now appear on the surface. The rearrangements of surface morphology seemed to create further fracture in the oxide layer, shown especially at high magnification. Also, a grainy texture appears after aging, whereas the surfaces were very smooth prior to aging. The ESCA data shown in Tables VII and VIII indicate very little change or difference in chemical composition. The comparisons between Tables VII and VIII show that in general the acid treatments have greater carbon content after aging whereas the Turco process decreased in carbon and increased in titanium.

In summary, surface treatment and aging cause profound changes in the surface morphology of Ti 6-4. The surface chemical composition remained remarkably constant, both in oxidation state and in stoichiometry. The most interesting feature was removal of about 50% of the carbon signal by cleaning in an argon discharge.

The surface morphology can be ranked in the order Turco>Pasa-Jell> phosphate/fluoride>anodize by considering the relative heights-of-asperities (or degree of three-dimensional development), and also the degree of change induced by aging. There appears to be a correlation with previous literature reports that claim basic treatments to be the least durable.

B. Adhesives (ESCA)

Last year we reported (1) that ESCA spectra obtained on the AEI equipment of known polymer structures gave excellent correlations for functionality and stoichiometry. During the current grant period, almost exclusive use was made of the DuPont 650 equipment. As mentioned earlier, this instrument provides rapid acquisition of data in the analog mode. Of particular interest to NASA are polyimides and their precursors, and polyphenylquinoxalines. Representative nomenclature, idealized structures,

and stoichiometry are shown in Table XII. ESCA spectra were reduced to binding energy, width at half-height, and atom fraction and these results listed in Table XIII.

Multiple valence states for carbon introduce overlapping peaks in the C 1s levels. Deconvolution (and more accurate data) are required to extract the important structure and bonding information in this region. Approximate position and intensity parameters are listed in Table XIII for partially resolved peaks in the 287-290 ev range deriving from carbonyl and carboxyl groups, and about 291 ev from aromatic shake-up satellites.

Structure-specific trends are more easily observed in the oxygen and nitrogen spectra. The oxygen peak widths average close to 3 ev in the molecules containing oxygen in two types of functional group, while widths are closer to 2 ev when the valence states are closer. Also the binding energy shifts at least 1 ev, going from the monomers to the polymer. It is not clear at this stage of analysis whether this is a primary chemical effect of amide and imide linkages or a secondary, inductive effect due to the close-packed polymer configuration. In PPQ, oxygen is an unexpected component, and may be due to residual carbonyl, water and/or solvent. The high binding energy is a further indication that a charging effect is occasioned by oxidation of the uppermost surface layer.

The nitrogen line widths reported in Table XIII are consistent and narrow, indicating that there is only one oxidation state in each of these materials. The binding energies show a decreasing trend, reflecting the change in oxidation state from $-NH_2$ to $-N(C=O)_2$ to $N=C$.

Atom fractions are calculated from peak intensities according to some

TABLE XII

IDEALIZED STRUCTURE AND COMPOSITION OF MONOMERS AND POLYMERS

	Stoichiometry, %		
	C	O	N
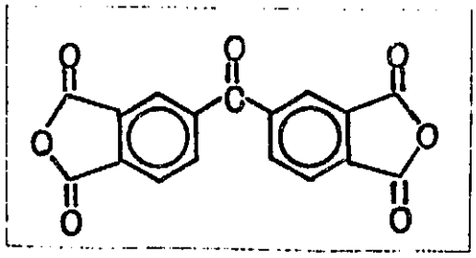	71	29	-
1. BDTA			
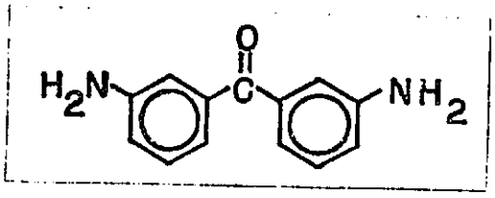	81	6	13
2. mm'-DABP			
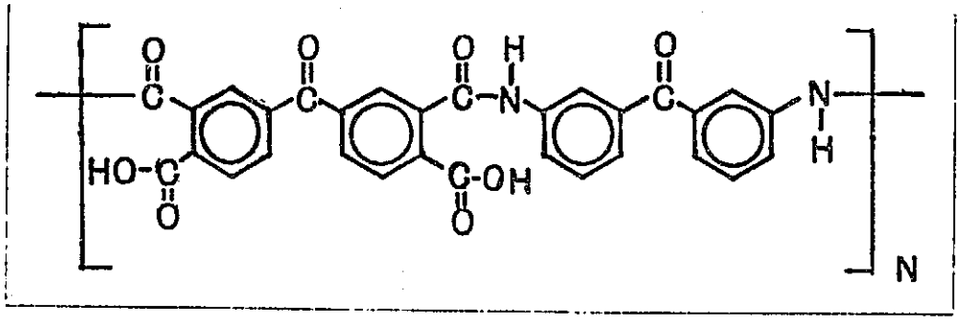	75	20	5
3. LaRC-2(polyamic acid)			

ORIGINAL PAGE IS
OF POOR QUALITY

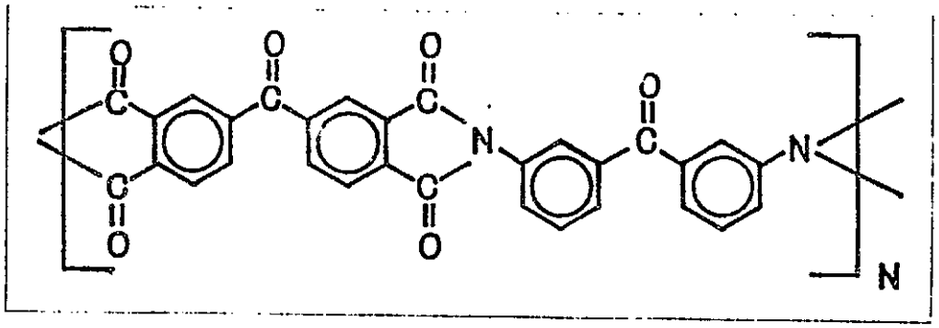	79	16	5
4 LaRC-2 (polyimide)			

	Stoichiometry,%		
	C	O	N
5. LaRC-13	81	14	5
6. Kapton	76	17	7
7. PPQ	89	-	11

ORIGINAL PAGE IS
OF POOR QUALITY

TABLE XIII

ESCA PARAMETERS FOR NASA-LaRC MONOMERS AND POLYMERS

	Compound	C 1s BE	C 1s I	C 1s W	O 1s BE	O 1s I	O 1s W	N 1s BE	N 1s I	N 1s W
1.	BDTA	285.0 289.1 291.0	59 16 5	2.1	532.4	21	3.0			
2.	mm'-DABP	285.0 290.7	73 7	2.3	532.0	13	2.9	403.3	14	1.9
3.	LaRC-2 (polyamic acid)	285.0 287.5 290.0	67 11 4	1.9	533.4	13	2.9	400.9	4	1.8
4.	LaRC-2	285.0 288.4 290.8	67 12 3	1.7	533.2	15	2.0	400.8	3	1.6
** 4A.	LaRC-2'	285.0 288.3 291.0	76 8 3	1.8	533.6	10	2.4	401.1	3	1.6
5.	LaRC-13	285.0 289.5 291.0	68 12 3	2.1	533.2	11*	2.3	401.1	6	2.1
6.	Kapton	285.0 288.5 291.0	67 11 3		533.3	14#	2.5	399.8	5	1.6
7.	PPQ	285.0 291.0	84 4	1.8	534.0	3	1.5	399.8	9	1.5

* O 1s shake-up at 540.5 ev, I = 10% main
\# O 1s shake-up at 539.3 ev, I = 5% main
** Duplicate run

very liberal assumptions: (1) samples are homogeneous and free of contamination, (2) spectrometer calibration constant is unity, (3) theoretically computed cross-section values are accurate, (4) peak-height and peak-area ratios are identical and (5) linear base-line can be subtracted to remove inelastic scattering contributions. Moreover, our approximate procedure for convoluted carbon peaks probably overestimates the total carbon. In view of all the potential error, the agreement is gratifying. In particular, note that the trends in oxygen and nitrogen intensities correlate with idealized structure calculations.

Some of these results were combined with data on other polymers and used as the basis for publications on qualitative analysis of polymer structure and bonding by ESCA. Copies of these manuscripts are in the appendix.

C. Fracture Surfaces (SEM/EDAX)

1. PPQ/Anodized Ti 6-4 and /NR150B2 or /Skybond 710 Composites

Figure 9 shows representative features of a lap shear sample prepared with Ti 6-4 anodized adherends and PPQ adhesive on scrim cloth. Low strength resulted after the joint was left for three days in boiling water and then tested at 561 K (550^{o}F). Failure was 90% "near-interfacial", as indicated on the left. The adhesive fractured vertically, leaving part on each adherend, and the "bare" areas are covered with thin flakes of primer that were drawn in the direction of stress. This ductile fracture is also seen in areas of bulk adhesive failure.

Representative views of two samples with anodized Ti 6-4 coupons as one adherend and NR=150B2 composites as the other adherend, and PPQ (unsupported) adhesive are shown in Figure 10. Both samples gave moderate strength when tested at room temperature. The Skybond 710 sample had a three day water boil, and showed about 60% failure in the composite surface,

FIGURE 9

Four magnifications (20X, 50X, 200X, 500X) of fracture surface of a PPQ 413 (on scrim cloth) Ti/ (anodized) joint tested at 561 K (550°F) after 3 days water boil.

FIGURE 9. Four magnifications (20X, 50X, 200X, 500X) of fracture surface of a PPQ 413 (on scrim cloth)/Ti (anodized) joint tested at 561 K (550°F) after 3 days water boil - 4.9MNm^{-2} (710 psi).

Several failure modes are: Ductile fracture in adhesive, fiber/adhesive interfacial failure, primer/adherend "interfacial" failure, leaving thin flakes of primer adhering.

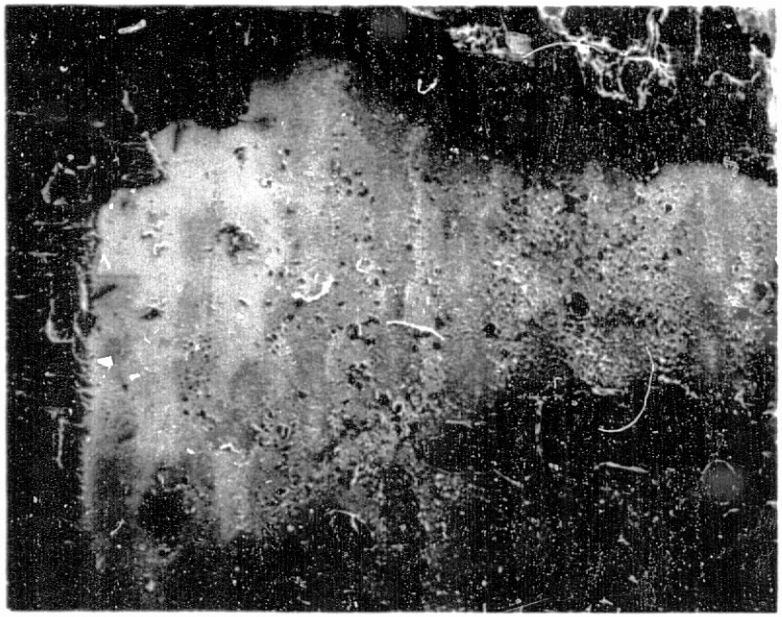

5mm

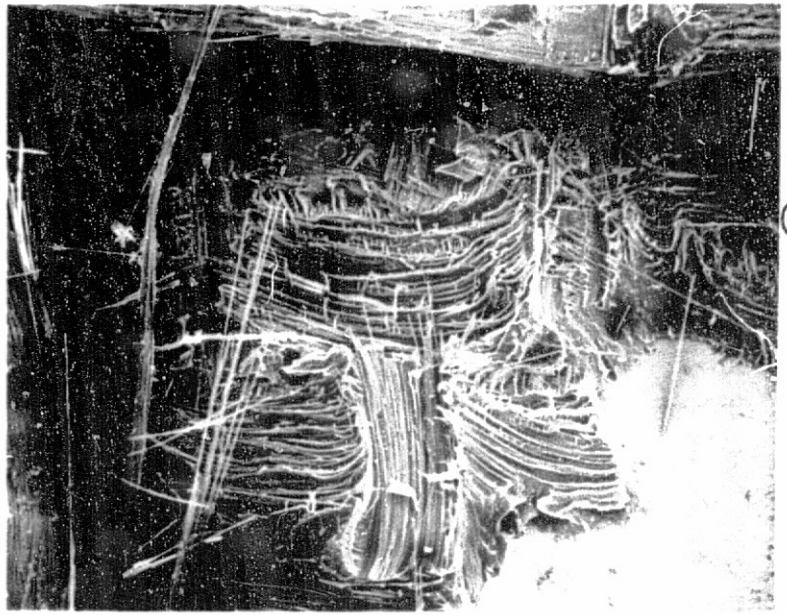

0.2 mm

ORIGINAL PAGE IS
OF POOR QUALITY

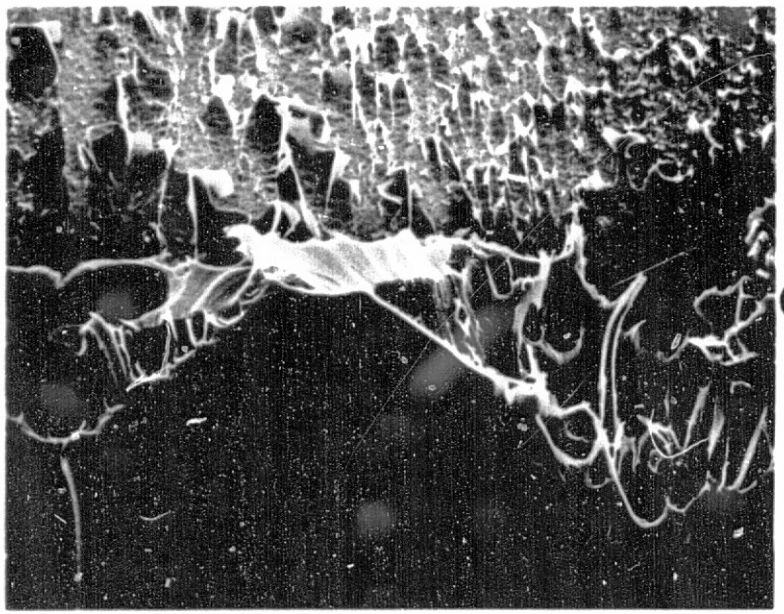

0.5mm

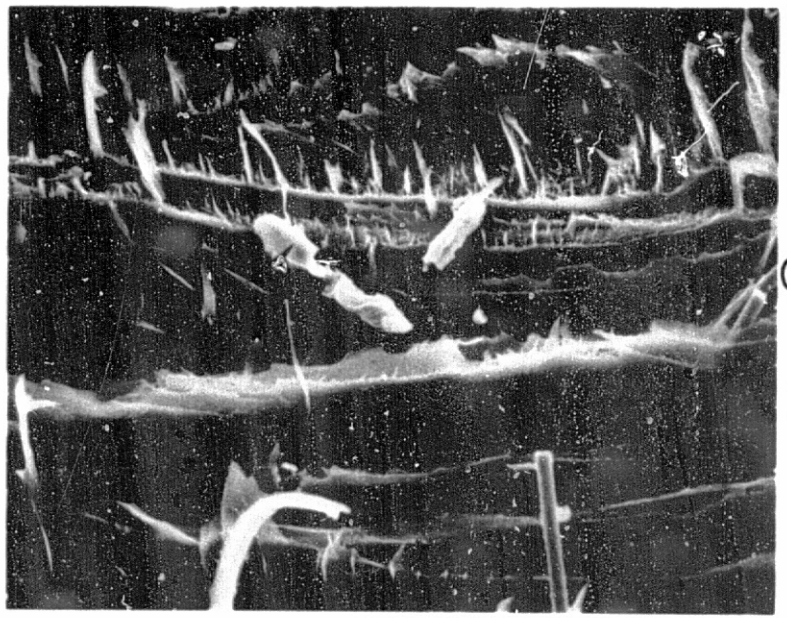

0.2 mm

FIGURE 10

Three magnifications (20X, 500X, 1000X) of fracture surface of a PPQ 413/Ti (anodized)/ NR-150B2-HTS composite joint tested at room temperature.

FIGURE 10. Three magnifications (20X, 2@ 500X, 1000X) of fracture surface of a PPQ 413/Ti (anodized)/NR-150B2-HTS composite joint tested at room temperature = 16.5MNm^{-2} (2400 psi).

(Bottom Left) one magnification (500X) of PPQ 413/Ti (anodized)/ Skybond 710-HTS composite tested at room temperature after three days water boil = 18.9MNm^{-2} (2750 psi). Both samples very similar. Ti surface has numerous dark "smudges" that are seen to be salt pits in the next two figures.

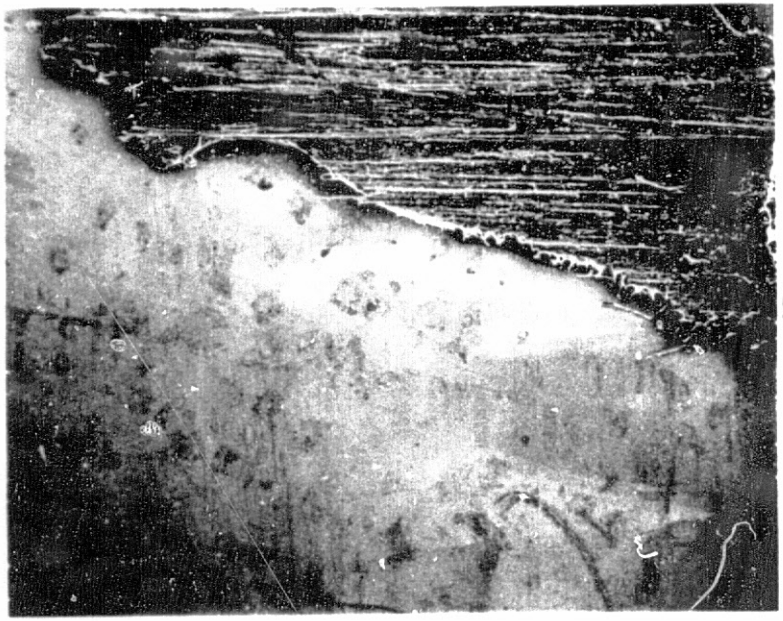

5mm

0.2mm

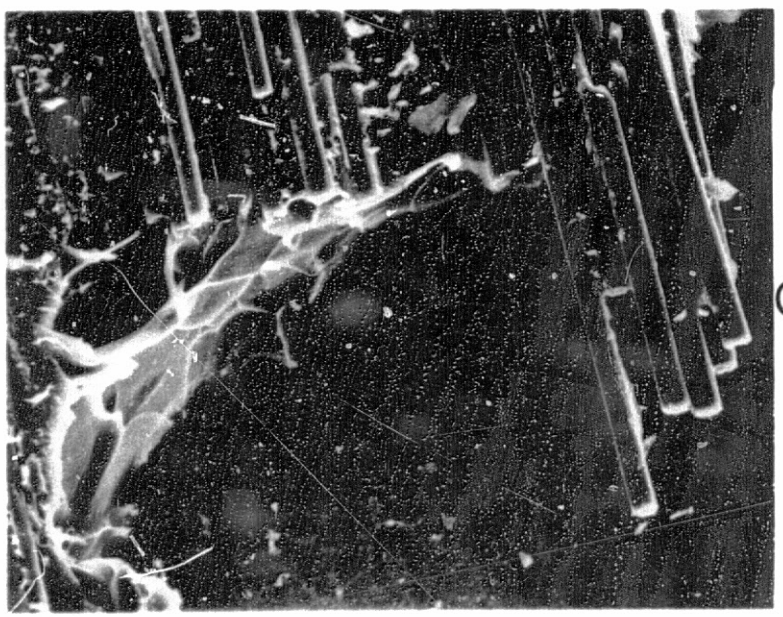

0.2mm

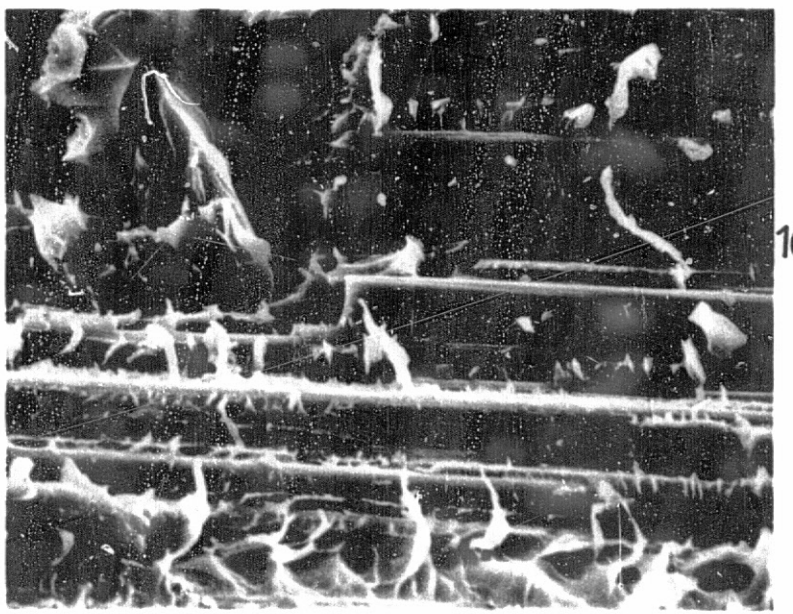

100 μm

ORIGINAL PAGE IS
OF POOR QUALITY

40% titanium interfacial, while the NR-150B2 showed > 80% failure at the titanium surface. In both instances, black "smudges" seen in the upper left photomicrograph appeared on the titanium surfaces. Higher magnification views of these anomalous, dark areas are shown in Figure 11, where they have features distinctive of corrosion pits. Indeed, EDAX analysis in Figure 12 shows that the crystal-like growths projecting up from the dark background are composed of sodium and potassium chloride.

2. LARC-13/Ti6-4 vs. Temperature and Al Filler

Figures 13-16 are rather similar, in keeping with the similarity in lap shear strength values. Interfacial failure and voids are the predominant features. Also, the adhesive-side of the interfacial failure replicates the adherend poorly, further indicating poor wetting and spreading in the glue line that probably contributed to void formation. The sample aged and tested at 588 K ($600^{o}F$) had the greatest proportion of bulk failure.

Considerably higher strength was obtained with the samples shown in Figures 17 and 18, and interfacial failure was decreased proportionally. The color of the "flash" was distinctly lighter, and even the adherends were lighter. The void content was quite similar however. The high filler content in the latter sample appeared to effect greater bulk fracture, thus improving strength at room temperature.

3. Composite Short Beam Shear Specimen

Previously we had used EDAX only occasionally on composite substrate samples. Usually the data showed only the Au/Pd coating: the lighter elements (below fluorine) are not detected by X-ray fluorescence. Occasionally, however, some extraneous element would appear. Now we have

FIGURE 11

Three magnifications (500X, 2 @ 1000X, 2000X) of adherend areas from the previous two samples.

FIGURE 11. Three magnifications (500X, 2 @ 1000X, 2000X) of adherend areas from the previous two samples.

These features look like corrosion pits and EDAX (Figure 12) shows the crystals to be sodium and potassium chloride.

0.2mm

100 μm

ORIGINAL PAGE IS
OF POOR QUALITY

50 μm

100 μm

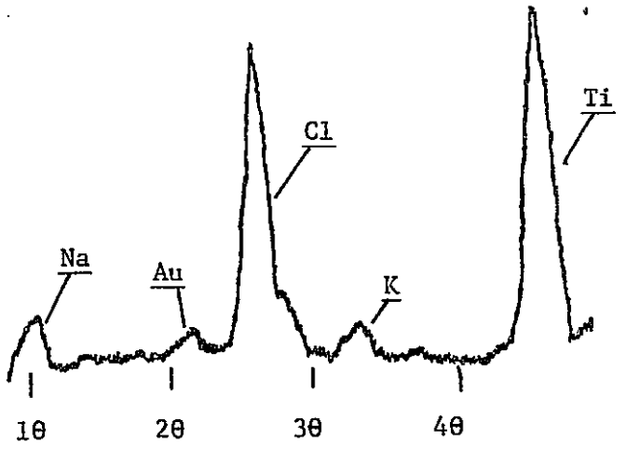

Figure 12. EDAX spectrum taken from corrosion pit in Figure 11

FIGURE 13

Three magnifications (20X, 100X, 2 @ 500X) of fracture surface of LaRC-13 (on scrim cloth)/Ti (phosphate fluoride) joint tested at room temperature.

FIGURE 13. Three magnifications (20X, 100X, 2 @ 500X) of fracture surface of LaRC-13 (on scrim cloth)/Ti (phosphate/fluoride) joint tested at room temperature = 12.2MNm^{-2} (1780 psi).

Interfacial failure and voids are roughly equivalent. Some brittle primer failure is apparent at high magnification.

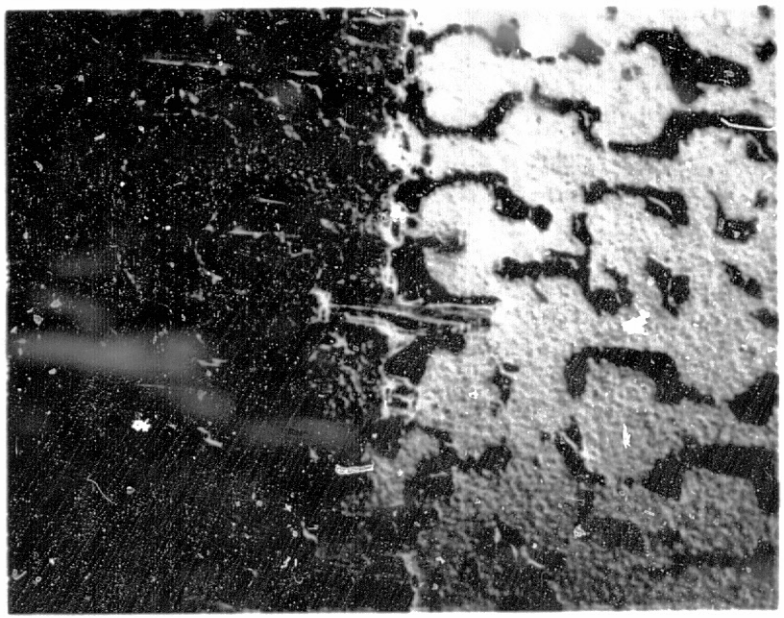

5mm

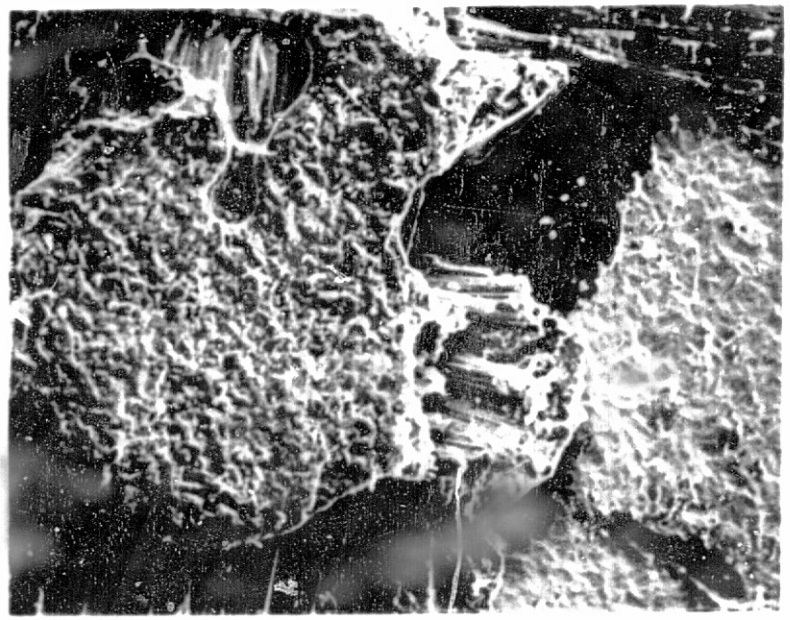

1 mm

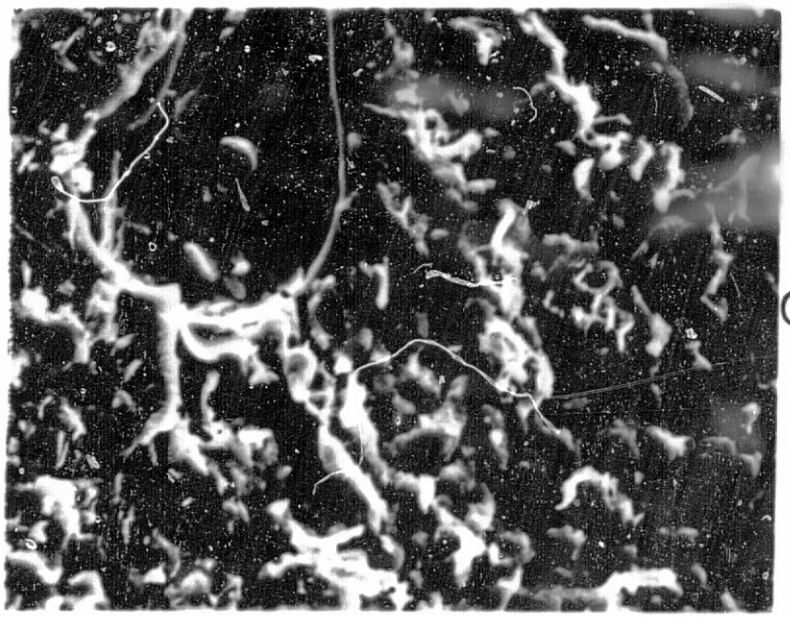

0.2 mm

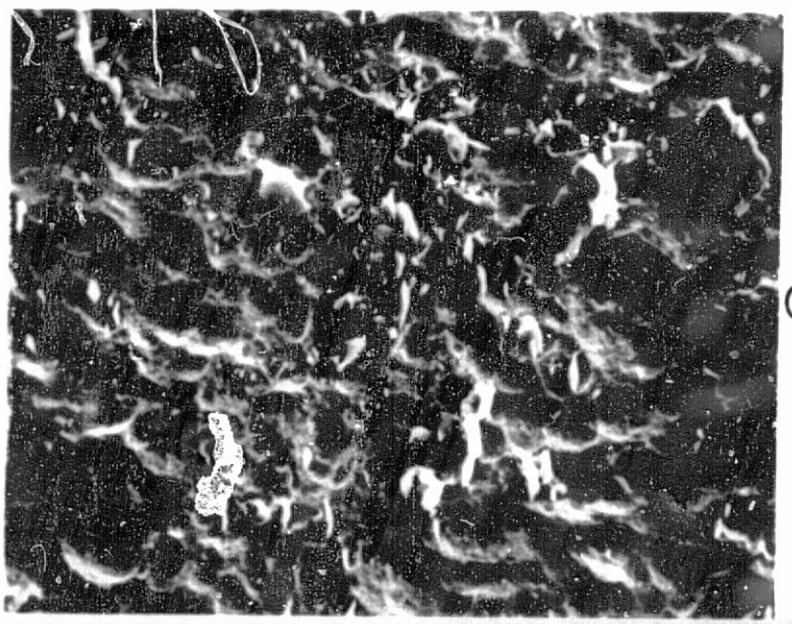

0.2mm

FIGURE 14

Three magnifications (20X, 100X, 2 @ 500X) of fracture surface of LaRC-13 (on scrim cloth)/Ti (phosphate/fluoride) joint tested at 589 K ($600^{\circ}F$).

FIGURE 14. Three magnifications (20X, 100X, 2 @ 500X) of fracture surface of LaRC-13 (on scrim cloth)/Ti (phosphate/fluoride) joint tested at 588 K (600°F)= $8.3 MNm^{-2}$ (1200 psi).

Void and interfacial failure predominate.

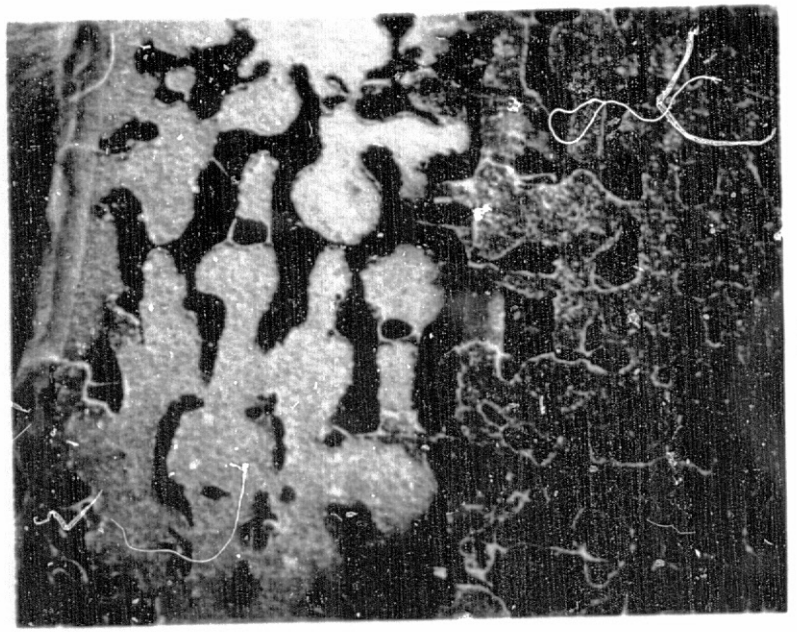

5mm

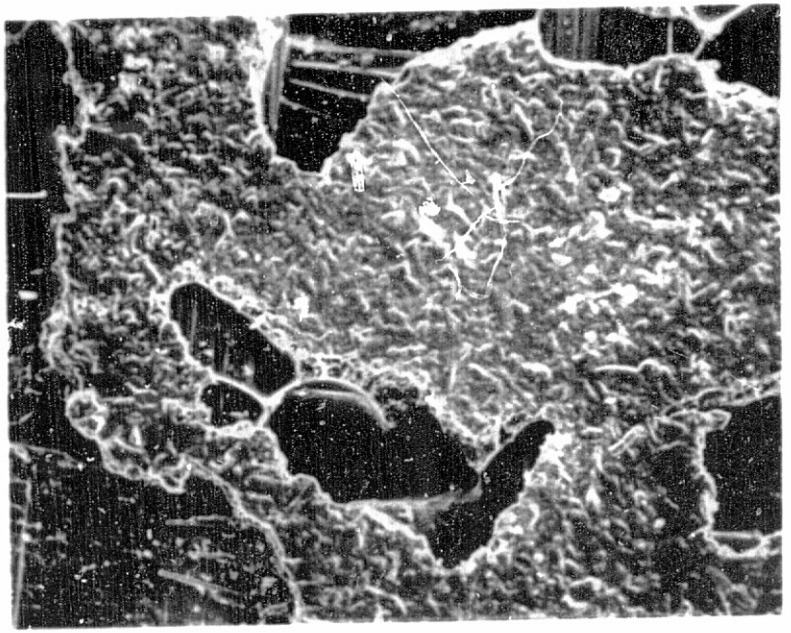

1 mm

ORIGINAL PAGE IS
OF POOR QUALITY

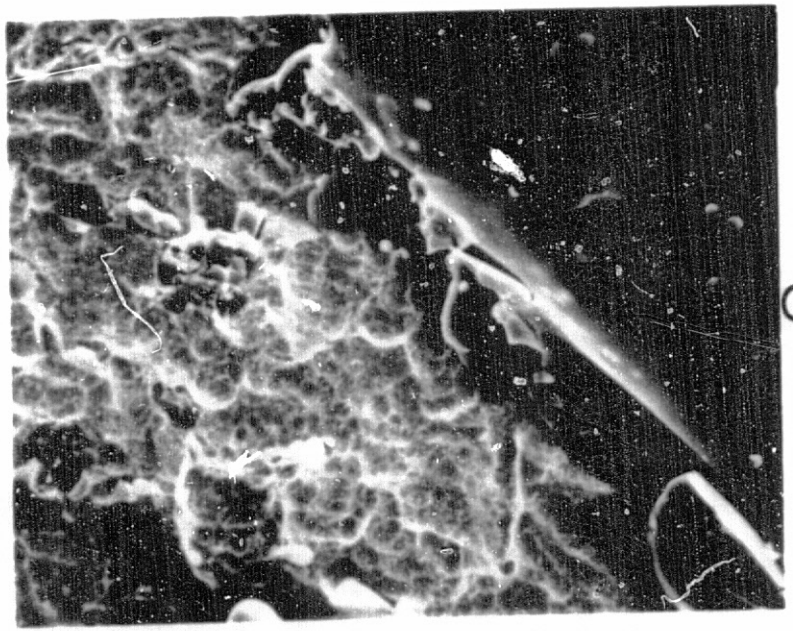

0·2 mm

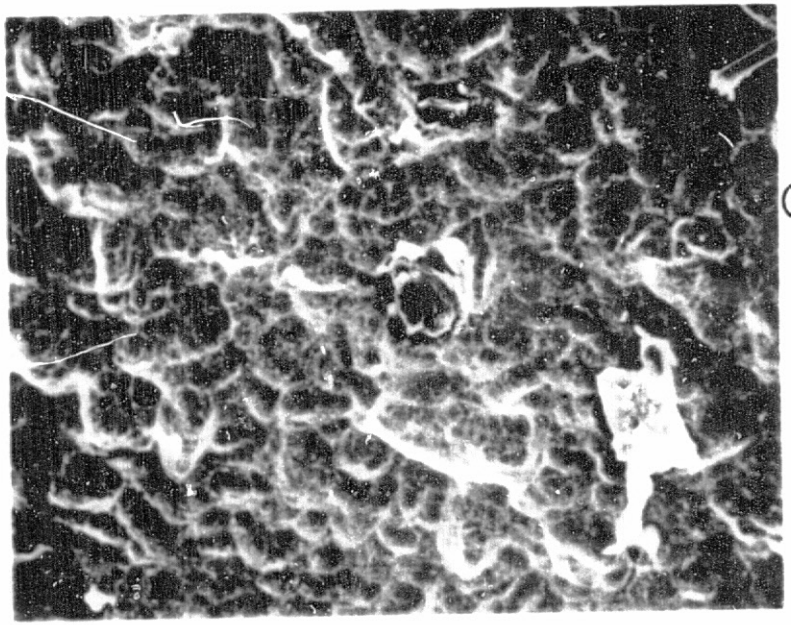

0.2mm

FIGURE 15

Three magnifications (20X, 100X, 2 @ 500X) of fracture surface of LaRC-13 (on scrim cloth)/ Ti (phosphate/fluoride) joint tested at room temperature after 125 hours aging at 589 K ($600^{o}F$).

FIGURE 15. Three magnifications (20X, 100X, 2 @ 500X) of fracture surface of LaRC-13 (on scrim cloth)/Ti (phosphate/fluoride) joint tested at room temperature after 125 hours aging at 588 K (600^{o}F) = 13.3MNm^{-2} (1940 psi).

Significant fiber/ratios fracture occurs and brittle primer louvers are left on titanium.

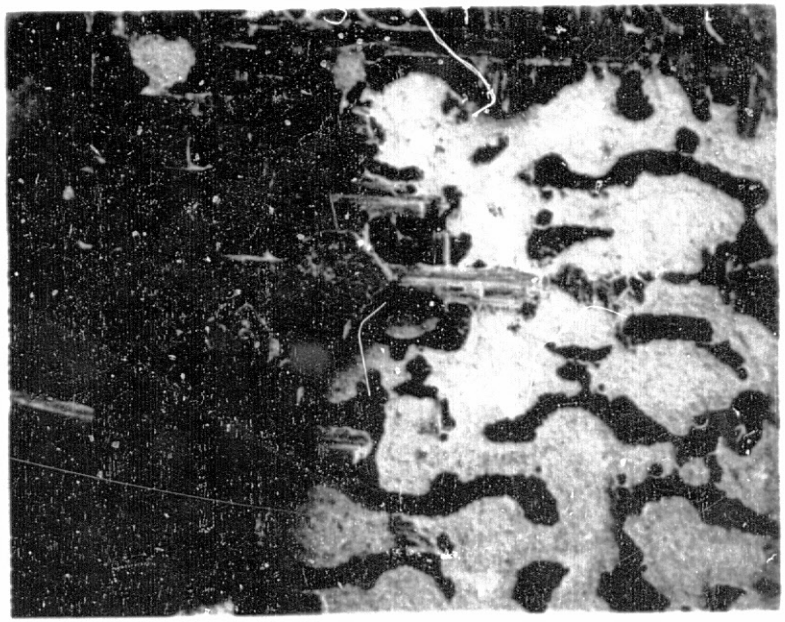

5mm

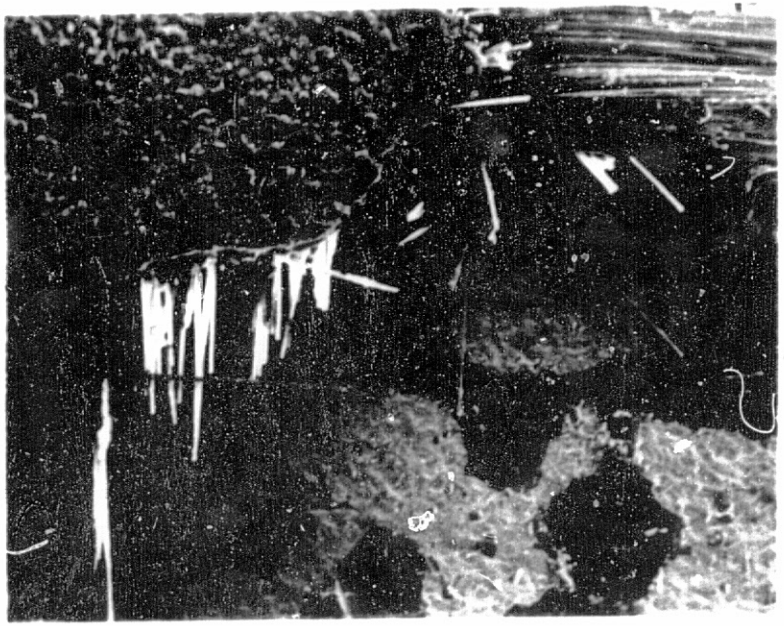

1mm

ORIGINAL PAGE IS
OF POOR QUALITY

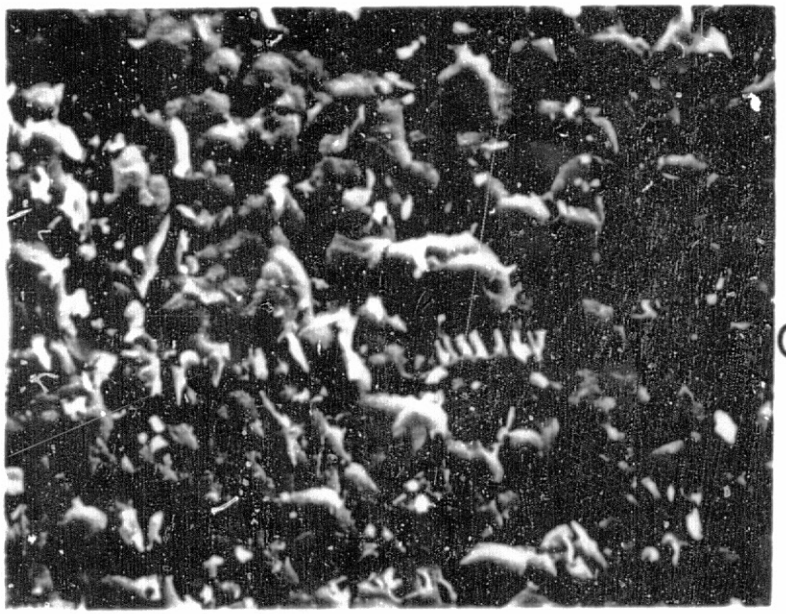

0.2mm

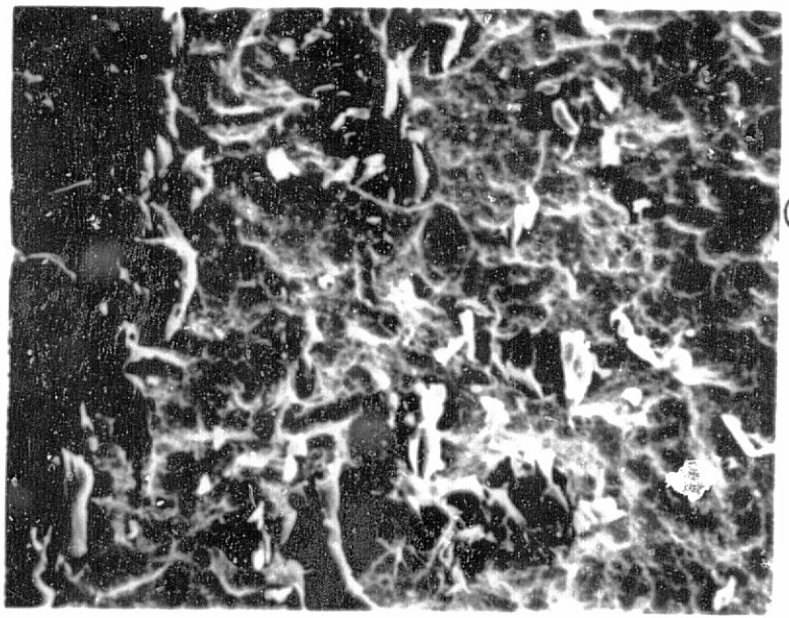

0.2 mm

FIGURE 16

Three magnifications (20X, 100X, 2 @ 500X) of fracture surface of LaRC-13 (on scrim cloth) / Ti (phosphate/fluoride) joint tested at 589 K (600°F) after 125 hours aging at 589 K (600°F).

FIGURE 16. Three magnifications (20X, 100X, 2 @ 500X) of fracture surface of LaRC-13 (on scrim cloth)/Ti (phosphate/fluoride) joint tested at 588K (600°F) after 125 hours aging at 588 K (600°F) = 12MNm^{-2} (1750 psi).

Matrix and fiber/matrix failure contribute to strength, but less brittle primer fracture occurs than in the last sample.

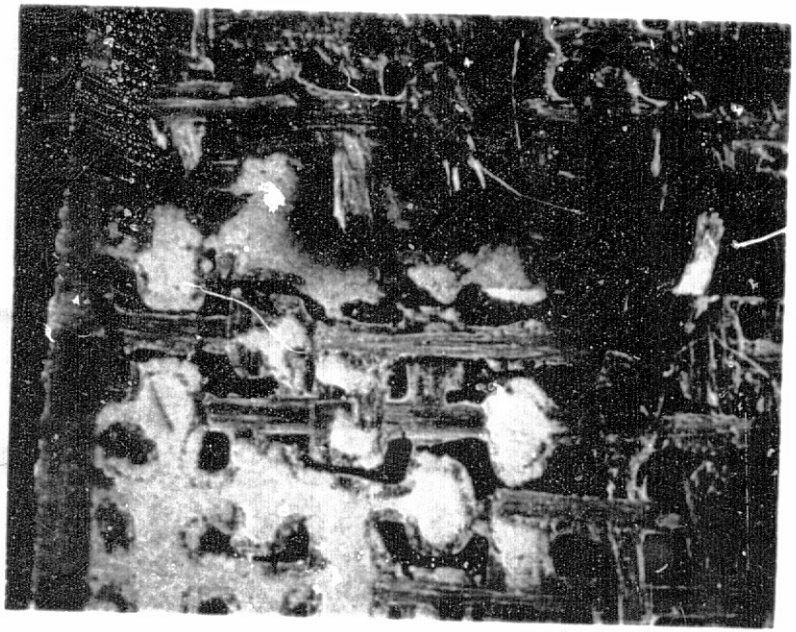

5mm

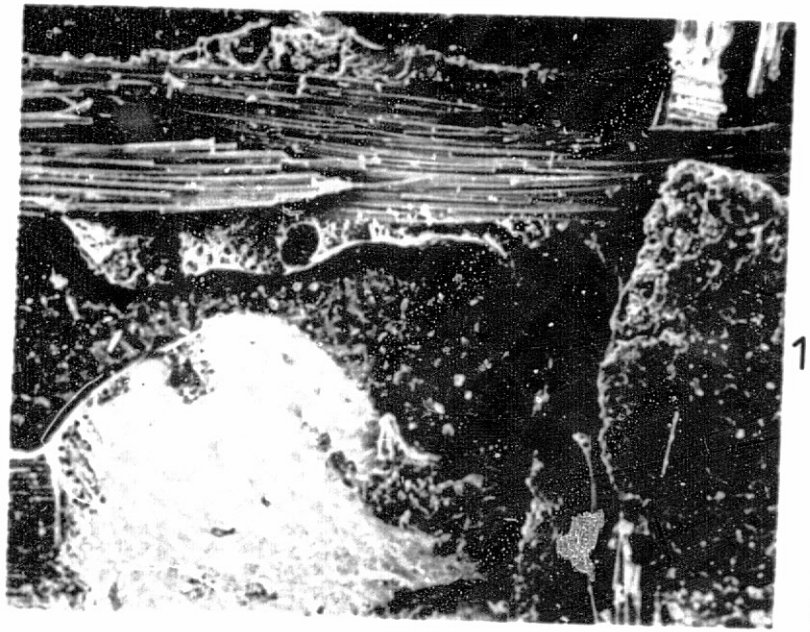

1mm

ORIGINAL PAGE IS
OF POOR QUALITY

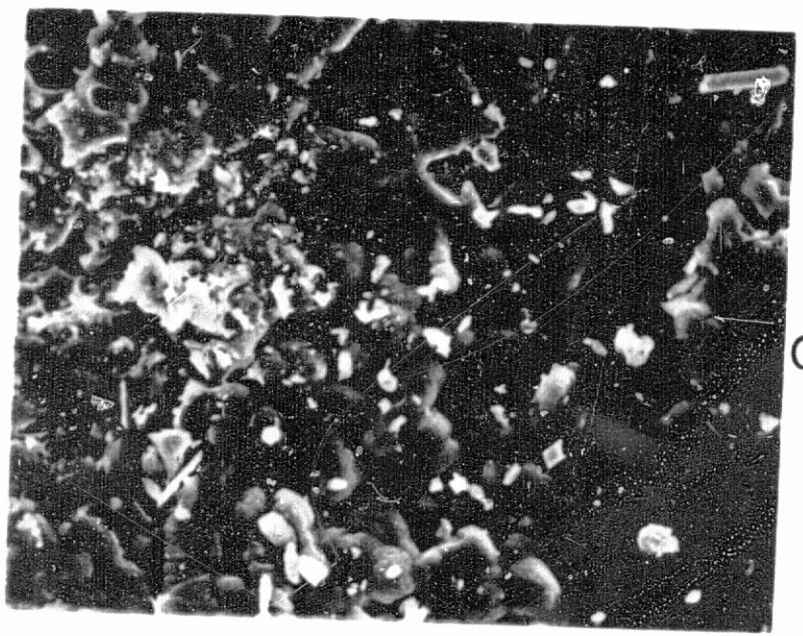

0.2mm

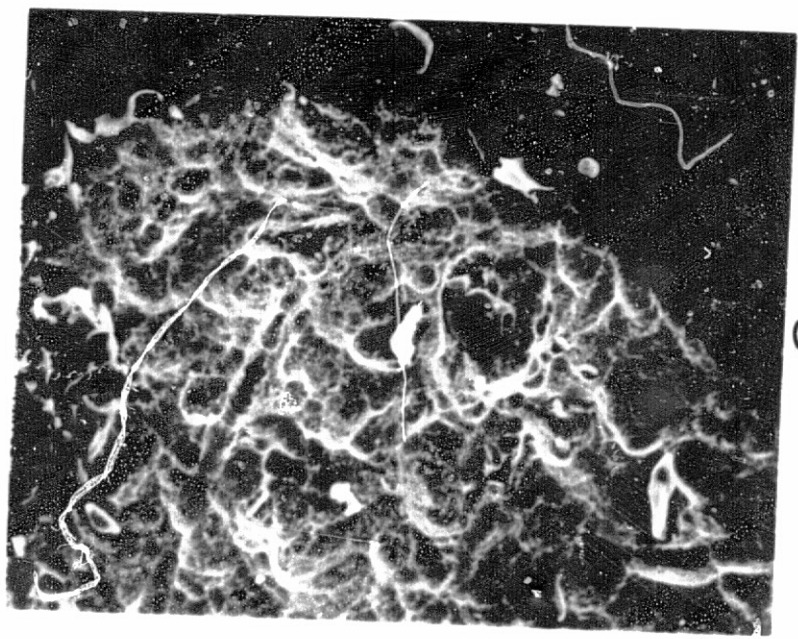

0.2mm

FIGURE 17

Three magnifications (20X, 100X, 2 @ 500X) of fracture surface of LaRC-13 (on scrim cloth) / Ti (phosphate/fluoride) joint tested at room temperature.

FIGURE 17. Three magnifications (20X, 100X, 2 @ 500X) of fracture surface of LaRC-13 on scrim cloth/Ti (phosphate/fluoride) joint tested at room temperature = 22MNm^{-2} (3200 psi).

Fiber/matrix, void and interfacial failure are mixed. Brittle louvers on adherend add to surface area of fracture.

ORIGINAL PAGE IS
OF POOR QUALITY

FIGURE 18

Three magnifications (20X, 100X, 2 @ 500X) of fracture surface of LaRC-13 (with 60% Al powder on scrim cloth)/Ti (phosphate/fluoride) joint tested at room temperature.

FIGURE 18. Three magnifications (20X, 100X, 2 @ 500X) of fracture surface of LaRC-13 (with 60% Al powder on scrim cloth/Ti (phosphate/fluoride) joint tested at room temperature = 24.5MNm^{-2} (3560 psi).

This is the only case where no titanium adherend appears, although void bottoms are primer. Extra fine micro structure, N5-20μm, seems associated with filler particles, and must be the source of high strength.

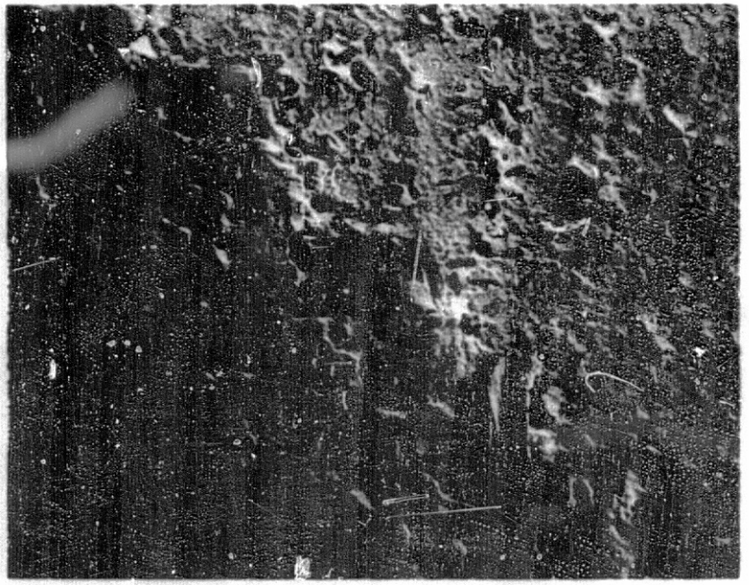

5mm

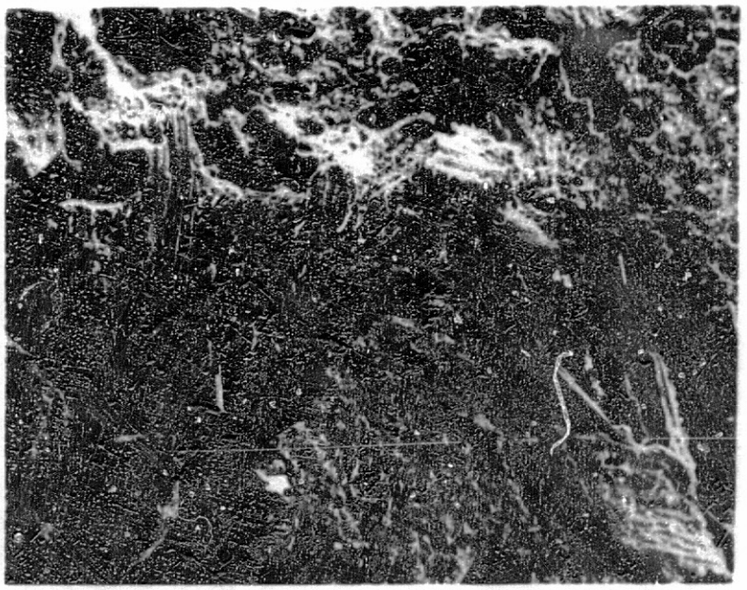

1 mm

ORIGINAL PAGE IS
OF POOR QUALITY

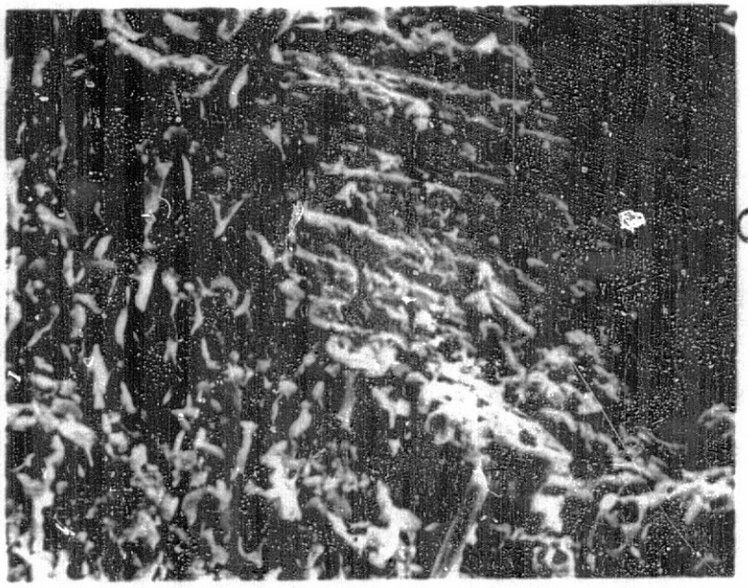

0.2mm

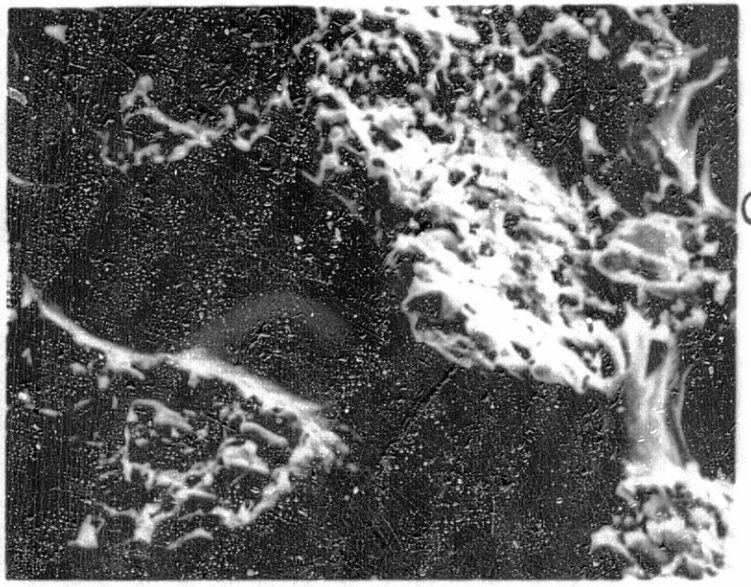

0.2mm

systematically examined cross-sections of HT-S graphite fiber composites with matrix polymers P13N, Skybond 710, NR-150B2 and PPQ. Generally, the presence of extraneous elements, such as our conjecture of silicon from mold release agents, has been ruled out. Rarely was any element detected, and never in a uniform concentration over any appreciable area, as would be expected in the case of diffusion of contamination.

Photomicrographs of a tested interlaminar (short beam) shear specimen are shown in Figure 19. The nature of the failure is more easily observed in the split cross-section at the bottom of the figure. This was the first such sample studied with the "scouting" objective to see whether any distinctive features could be determined on these small difficult-to-handle specimens. More samples with different strength values would need to be examined to find whether SEM could be predictive or diagnostic for strength.

4. Rubber-Toughened Epoxy

In Figures 20 and 21, scanning electron micrographs illustrate the fracture of epoxy resin with and without rubber-toughened additives. Immediately obvious is a relative uniform dispersion of particles in one case and a bimodal dispersion of smaller particles in the second rubber-toughened sample. This illustrates the utility of SEM fractography for the study of microphase-separated polymers systems. The relative size distribution of the dispersed phase is clearly revealed. Further the number and size of rubber inclusions correlate with fracture toughness and fractography provides insight into microscopic failure and toughening mechanisms. It appears that cracks proceed through the brittle, epoxy matrix and two possible processes occur at the spherical inclusions of the CTBN rubber phase. In the more predominant case, fracture proceeds

FIGURE 19

Two magnifications (200X, 500X) of outside (top) and inside (bottom) of a PPQ (1:3) SRI2 interlaminar shear specimen tested at 561 K (550°F).

FIGURE 19. Two magnifications (200X, 500X) of outside (top) and inside (bottom) of PPQ (1:3) SRI2 interlaminar Shear specimen tested at 561 K ($550^{o}F$) = 35.8MNm^{-2} (5200 psi).

Shown most clearly in the interior view (Bottom), a section about 0.1 mm wide has separated from the center just above the pressure edge.

0.5mm

0·2mm

0.5mm

0.2mm

ORIGINAL PAGE IS
OF POOR QUALITY

FIGURE 20

Two magnifications (2000X, 10,000X) of an epoxy resin fracture surface.

FIGURE 20. Two magnifications (2000X, 10,000X) of an epoxy resin fracture surface.

It is through the development of high surface area by brittle cleavage, both parallel and perpendicular to the direction of fracture, that give toughness and strength to epoxy adhesives.

ORIGINAL PAGE IS
OF POOR QUALITY

FIGURE 21

Two magnifications (200X, 10,000X) of a fractured monodisperse rubber toughened epoxy sample and of a bimodal dispersed rubber toughened epoxy sample.

FIGURE 21. Two magnifications (200X, 10,000X) of A. a fractured monodisperse rubber toughened epoxy sample and B. bimodal-dispersed, rubber toughened epoxy sample.

The matrix resin in these two samples is the same as in Fig. 20. However, both samples of CTBN toughened epoxy show higher strength and fracture toughness values. A. shows that the CTBN rubber phase was dispersed relatively uniformly in particles sizes of approximately one μm diameter. In Side B a bimodal distribution appears with the larger particles averaging approximately 0.5 μm in diameter and the smaller particles ranging about 0.1 μm in diameter. These photomicrographs clearly show the analytical capability to study microphase-separated polymer structure by SEM fractography.

ORIGINAL PAGE IS
OF POOR QUALITY

around the particle in the matrix, and the particle is subsequently stretched as the crack expands. Finally the stretched rubber particle breaks, leaving "stringy" residue at the bottom of the cavities in the matrix, and some scattered particulate debris. Fine cracks frequently extend into the matrix from the perimeter of the cavities, indicating significant strains are induced by the rubbery response of the dispersed phase. The bimodal, smaller distribution has greater quantities of these mechanisms, and is therefore tougher. The second mechanism that occurs in the toughened epoxies is a direct transmission of the brittle crack through the rubber phase, in some cases with a slight deflection out of plane. This mechanism probably contributes relatively little to toughening.

IV. SUMMARY AND CONCLUSIONS

Scanning electron microscopy/Energy dispersive analysis of X-rays (SEM/EDAX) results on NASA-LaRC materials elucidated changes in the morphology of Ti 6-4 oxide layers, identified contaminants and other failure nuclei, and displayed a variety of microscopic mechanism accompanying fracture in adhesives and composite adherends. Complementary information from X-ray photoelectron spectroscopy (ESCA) added details on oxidation states at the uppermost surface in both metallix and polymeric materials. In the latter, the potential of ESCA was demonstrated for rapid qualitative analysis and monitoring of chemical changes caused by processing.

Stepwise, titanium 6-4 alloy was characterized as received, after grit blasting and subsequent etching by the following processes: (i) anodize, (ii) phosphate/fluoride, (iii) Pasa-Jell and, (iv) Turco, and then thermo-oxidative aging. Basic electron spectroscopic data were collected for polyimide and polyphenylquinoxaline adhesives and synthetic precursors. Fractographic studies were completed for several combinations of adherend, adhesive and testing conditions. The following specific conclusions may drawn from the results obtained during the current grant period:

1. Ti 6-4 has totally different morphology on opposite sides before grit blasting. One side has markings that appear to be the result of process working or subsequent deburring.

2. Grit blasting destroys the original structures, leaving the surface heavily worked and fragmented and covered with minute fracture debris. Aluminum content is significantly increased although uniformly

and no Al_2O_3 grit blast particles appear.

3. Each of the four chemical surface treatments produced unique surface morphology, with only the two acid treatments bearing any resemblance to each other.

4. A qualitative ranking: Turco > Pasa-Jell >phosphate/fluoride > anodize was made both by considering the degree of roughness and the degree of change in surface morphology after 505 K (450°F) exposure in air.

5. Oxidation states and chemical composition revealed by ESCA was remarkably uniform, independent of treatment, except for trace constituents apparently adsorbed from treatment baths.

6. Some oxide layers were very thin because titanium (0) metal signal was obtained by ESCA.

7. Oxidation generally seems to diminish the size of surface structures and to favor the alpha phase at the expense of the beta phase.

8. ESCA provided rapid qualitative analysis of the monomers and polymers of interest to NASA-LaRC. Chemical shifts, especially in oxygen and nitrogen levels, provided correlations with structural features.

9. Interfacial failure dominated the PPQ/anodized Ti 6-4 lap shear strength specimens. Salt pits were found on the alloy indicating corrosion proceeded under the bond.

10. LaRC-13 samples also showed considerable interfacial failure apparently initiated by a large number of voids. From the large "flash" volume, it seems that there is high flow of adhesive out of the joint.

11. Addition of Al filler particles minimizes these difficulties. Moreover, the particles act as nuclei for high area drawing and fracture, further improving strength at room temperature.

V. REFERENCES

1. D. W. Dwight and J. P. Wightman, "A Fundamental Approach to Adhesion: Synthesis, Surface Analysis, Thermodynamics and Mechanics," Final Report, NASA Grant NSG-1124, VPI & SU, February, 1977.

2. D. W. Dwight, J. E. McGrath and J. P. Wightman, "ESCA Analysis of Polymer Structure and Bonding. I," Polymer Preprints 18 (2), 123 (1977).

3. R. F. Muraca and J. S. Whittick, "Materials Data Handbook on Titanium 6Al-4V," NASA Tech Brief B73-10372, October 1973.

4. ASM Committee on Metallography of Titanium and Titanium Alloys, "Microstructure of Titanium Alloys," Metals Handbook, 7, 321 (1972).

5. N. L. Rogers, "Surface Preparation of Metals for Adhesive Bonding," Applied Polymer Symposia 3, 327 (1966).

6. W. C. Hamilton, "Some Useful Techniques for Characterization of Adherend Surfaces," Applied Polymer Symposium 13, 105 (1972).

7. Earl D. Newell and Gilberto Carrillo, "A new Surface Preparation Process For Titanium," Materials and Processes for the 1970's, SAMPE Conference, 1973, p. 131.

8. R. H. Shoemaker, "New Surface Treatments for Titanium," Titanium Science and Technology, 4, 2401 (1973).

9. A. Benninghoven, H. Bispinck, O. Ganschow, and L. Wiedmann, "Quasisimultaneous SIMS-AES-XPS investigation of the oxidation of Ti in the monolayer range," Applied Physics Letters, 31, 341 (1977).

10. K. W. Allen, and H. S. Alsalim, "Titanium and Alloy Surfaces for Adhesive Bonding," J. Adhesion, 6, 299 (1974).

11. Motte, C. Coddet, P. Sarrazin, M. Azzopardi, and J. Besson, "A Comparative Study of the Oxidation with Water Vapor of Pure Titanium and of Ti6 Al-4V," Oxidation of Metals 10, 113 (1976).

12. F. Dalard, C. Montella et J. C. Sohm, "Adhension Des Peintures Sur Le Titane Anodise," Surface Technology 4, 367 (1976).

13. H. D. Shih and F. Jona, "Low-Energy Election Diffraction and Auger Electron Spectroscopy Study of the Oxidation of Ti (0001) at Room Temperature," Applied Physics 12, 311 (1977).

14. C. Coddet, "ESSAI DINTERPRETATION DU mechanisme D'OXYDATION DE L'ALLIAGE DE TITANE TA6V4 PAR L'OXYGENE SEC ENTRE 700°C ET 1000°C," Journal of the Less-Common Metals 51, 1 (1977).

15. R. A. Gledhill and A. J. Kinloch, "Environmental Failure of Structural Adhesive Joints," Journal of Adhesion 6, 315 (1974).

16. M. Gettings, F. S. Baker, and A. J. Kinloch,"Use of Auger and X-ray Photoelectron Spectroscopy to Study the Locus of Failure of Structural Adhesive Joints", Journal of Applied Polymer Science 12 (2) 375 (1977).

17. P. M. Stifel, "Durability Testing of Adhesive Bonded Joints," New Industries and Applications for Advanced Materials Technology, SAMPE Publin., Azusa, CA, 1974 p. 75.

18. T. Smith and D. H. Kaelble, "Mechanism of Adhesion Failure Between Polymers and Metallic Substrates: Al 2024-T3 and Ti 6-4 with HT 424 Adhesive," Report No. 74-73, Air Force Materials Laboratory, Wright-Patterson Air Force Base, Ohio (1974).

19. R. F. Wegman, "Durability Testing of Adhesive Bonded Joints," Applied Polymer Symposium 19 384 (1972).

20. F. Wegman and J. Bodnar, "Structure Adhesive Bonding of Titanium - Superior Surface Preparation Techniques," Quarterly 5, 28 (1973).

21. D. W. Levi, R. F. Wegman, and M. J. Bondar, "Effect of Titanium Surface Pretreatment and Surface Exposure Time on Peel Strength of Adhesive Bonds," SAMPE Journal, March/April, 32, (1977).

22. W. C. Jones III, E. McAbee, R. F. Wegman, and D. W. Levi, "Use of Multiple Regression Analysis to Develop Predictive Models for Failure Times of Adhesive Bonds at Constant Stress," Journal of Applied Polymer Science 18, 555 (1974).

23. K. Siegbahn, et al., "ESCA - Atomic, Molecular and Solid State Struture Studies by Means of Electron Spectroscopy", Almquist and Wiksells, Uppsala, 1967.

24. J. H. Scofield, "Hartree-Slater Subshell Photoionization Cross-Sections at 1254 and 1487 ev". J. Elec. Spectrosc. and Related Phenomena, 8 129 (1976).

25. Wightman, "The Use of SEM, ESCA and Specular Reflectance IR in the Analysis of Fracture Surfaces in Several Polyimide/Titanium 6-4 Systems", in Adhesion Science and Technology.

VI. ACKNOWLEDGEMENTS

Most of the work described in this report was performed on samples supplied by personnel in the Polymer Group at NASA-LaRC. Our studies would not have been possible without their efforts, especially Dr. Terry L. St. Clair and Mr. Paul Hergenrother in polymer synthesis and Ms. Anne K. St. Clair and Mr. Don Progar in adhesive testing. Also gratefully acknowledged is the expert SEM operation of Mr. Frank Mitsianis.

VII. APPENDIX

Paper 1 - "ESCA Analysis of Polymer Structure and Bonding. I." David W. Dwight, James E. McGrath and James P. Wightman, Polymer Preprints, 18,(2) 123 (1977).

Paper 2 - "ESCA Analysis of Polymer Structure and Bonding. I." David W. Dwight, James E. McGrath and James P. Wightman, Journal of Applied Polymer Science: Applied Polymer Symposia, "Polymer Analysis", J. Mitchell and T. K. Wu, Editors, Wiley-Interscience, New York, N. Y., 1978. (in press)

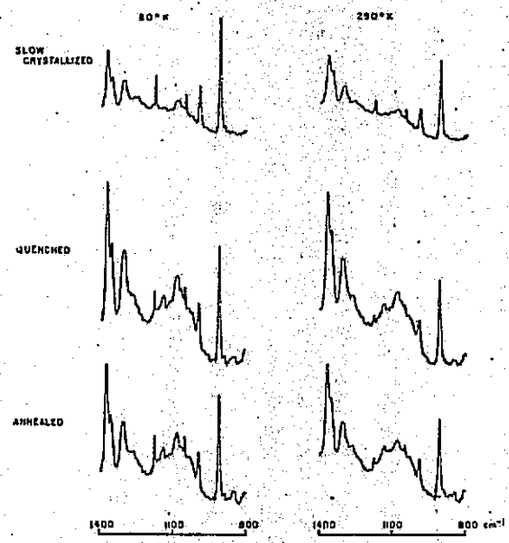

Fig. 1. Normalized peak height of 731 cm^{-1} absorption vs. temperature. (Data is offset for clarity.)

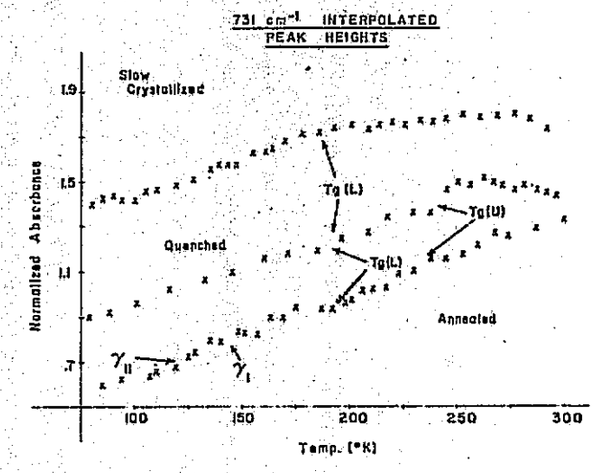

Fig. 2. Conformationally sensitive region of polyethylene spectrum at temperature extremes.

ORIGINAL PAGE IS OF POOR QUALITY

ESCA ANALYSIS OF POLYMER STRUCTURE AND BONDING. I.

David W. Dwight, James E. McGrath and James P. Wightman
Department of Chemistry
Virginia Polytechnic Institute and State University
Blacksburg, Virginia 24061

X-ray photoelectron spectroscopy (ESCA) provides rapid analysis of diverse polymer samples that can vary from experimental solutions to commercial films. The binding energies and intensities of core-level peaks identify the atoms and functional groups in the sample surface (~ 30 Å deep). Unsaturated systems give rise to "shake-up satellite" structures characteristic of local π-bonding. Spectra from a variety of polymers are presented to illustrate some of the potential of ESCA analysis.

INTRODUCTION

Engineering applications for synthetic polymers continue to expand; research and development directed toward defining new properties and processes and elucidating structure-property relationships is critical (1-5). Our previous work emphasized high-performance thermoplastics(6-8) and thermosets (9,10), and characterization of bulk physical properties such as thermal stability, dynamic mechanical behavior, toughness and adhesive-bond strength was of primary importance. ESCA was used mainly for chemical analysis of thin surface layers with composition different from the bulk (11,12).

Clark and co-workers published a series of papers pioneering fundamental ESCA studies of polymers(13). Measurements were made on well characterized, homogeneous polymers and model compounds. The results were correlated with non-empirical, CNDO/2 SCF Molecular Orbital calculations. Their work established that absolute and relative binding energies, and relative peak areas (intensities) are capable of elucidating many important aspects of polymer-surface chemistry.

Another level of information is available in aromatic-containing polymers; $\pi \rightarrow \pi^*$ transitions give rise to low-intensity "shake-up satellite" structures that are characteristic of the local π-bonding in repeat units (14). Clark, et al., applied this background information to a variety of problems including copolymer composition and structure, structural isomerism, and surface-fluorination kinetics(15).

Other workers have reported primarily fluoropolymer data, since the large chemical shift caused by fluorine substitution facilitates interpretation of the carbon 1s spectra (16). In these systems, ESCA has unique capability to study plasma-polymerized films(17), surface treatments and surface-segregation(11,12).

Included in our current study are commercial, engineering polymers and experimental copolymers from a variety of classes: polyimide, polycarbonate, polyester, polyarylene ether sulfone, polyarylene ether sulfide-sulfone, and polyphenylene oxide. The data show that each polymer system has a distinct ESCA "fingerprint", indicating the potential for rapid, semi-quantitative analysis. Moreover, shake-up satellites may provide new insight into structure and bonding in aromatic-containing polymers.

Polymer Prep. (ACS Div. Polym. Chem.)

EXPERIMENTAL

Apparatus

Initial ESCA data were collected on an AEI ES-100 photoelectron spectrometer using an aluminum anode and digital data acquisition. A digital PDP-8e computer/plotter was used to deconvolute and display the spectra. Recently we repeated the experiments on a DuPont 650 photoelectron spectrometer with a magnesium anode and direct display of the spectra on a strip-chart recorder. This system provided analysis of polymer samples in minutes. This is, of course, a significant advantage for routine work even though computer analysis must be added later. We are working on more detailed comparisons but the qualitatively distinctive features of polymers are basically the same in both spectrometers.

Materials and Procedures

Commercial grade films of "Mylar" polyester and "Kapton" polyimide were obtained from DuPont. "Lexan" polycarbonate and "Noryl" polyphenylene oxide were obtained as powders from General Electric. Extruded pellets of polysulfone were obtained from Union Carbide. Both polycarbonate and polysulfone were dissolved in chloroform and examined as cast films. Polyamic acid was cast as a thin film from 15% diglyme and imidization subsequently was accomplished by heating in air for one-hour at 100°, 200° and 300°C. The polythiosulfone (PSF-T) was prepared as described in detail elsewhere (8), and examined as a film cast from chloroform. The monomers bisphenol A and dichlorosulfone were obtained from Union Carbide. Crown Zellerbach supplied the 4,4'-thiodiphenol (Bisphenol T) and 4,4'-sulfonyl diphenol (Bisphenol S).

RESULTS AND DISCUSSION

Interpretation of ESCA spectra of polymers first assumes that effects are localized, and thus characteristic of the repeat unit. The functional constituents are identified by detailed comparison of the spectra with known reference standards or model compounds (monomers). More applications will arise now that the first correlation diagram for carbon 1s levels in polymers as a function of electronic environment has appeared (13). Relatively small chemical-shift effects often result in overlapping of peaks; deconvolution of such spectra aids in identifying the type and amount of functionality. For example, the carbon 1s levels of "Mylar" polyethylene terephthalate are shown in Fig. 1. The four component peaks (dotted lines) add together to exactly match the experimentally determined envelope (solid line). Separation of the ether-, carbonyl-, and aromatic-type carbons and rough estimate of their stoichiometry (1:1:3) are facilitated by deconvolution. However, our AEI digital data acquisition and interactive-computer analysis is relatively time consuming. Figures 2-4 show the results from several polymers and monomers, as obtained in the analog mode with the DuPont spectrometer. For routine analyses the ability to obtain ESCA spectra in minutes may be a significant advantage.

Comparison of Fig. 1 and Fig. 2A shows the same information in the carbon 1s levels as measured by each spectrometer. A shake-up satellite characteristic of π-bonding appears as a high-energy shoulder on the carboxyl peak at higher sensitivity. The oxygen levels are almost resolved into separate peaks for carbonyl- and ether-oxygens, and a shake-up satellite can just be distinguished from the background. Polyphenylene oxide shows relatively intense shake-up satellites in

both carbon and oxygen levels (Fig. 2B). The high-energy (low-intensity) peak in the polycarbonate carbon 1s levels (Fig.2C) is the combination of shake-up and carbonate peaks. The broad oxygen peak indicates two types of oxygen that differ in environment a little less than the oxygens in "Mylar". One would expect a shake-up satellite but the response was apparently below the signal-to-background ratio. The Bisphenol A model compound spectra in Fig. 2D helps provide confidence in interpretation of spectra of polymers derived from that monomer.

Fig. 3 shows three similar structures that are separated by ESCA. The phenyl-ether link in "Kapton" polyimide (Fig. 3A) results in the broadest carbon and oxygen main peaks, but the carbonyl peak (~289eV) is the narrowest. The potential to follow the thermal cure of polyamic acid to polyimide emerges from Fig. 3B and 3C. The presence of carboxyl groups in the amic acid has a broadening effect on the higher-energy carbon peak and the oxygen levels.

Oxidation of sulfur from thio- to sulfonyl- form produces a distinct chemical shift of about 5 eV, as shown by the model compound spectra in Fig. 4C and 4D. Analysis of polymers for the presence of either of these linkages is straightforward, as illustrated in Fig. 4B. In this case the objective was to obtain an equal number of each. The two oxidation states of oxygen give rise to broad oxygen levels in Fig. 4A and 4B, but curiously do not in 4D.

We are working on more accurate determination of ESCA peak shapes plus deconvolution routines for thorough characterization of structure and bonding in these and other polymer systems.

ACKNOWLEDGEMENT

The authors would like to thank NASA and ARO for their support of this research under NSG-1124 and DAAG-76-G0312.

REFERENCES

1. "Engineering Design for Plastics", E. Baer editor, S.P.E. Series 104 1964.

2. "Injection Molding of Engineering Thermoplastics", S.P.E. Series 306, June 1977.

3. "The Physics of Glassy Polymers", R. N. Haward Editor, Wiley (1973).

4. "Block Copolymers: Overview and Critical Survey", A. Noshay and J. E. McGrath, Academic Press (1977).

5. "Engineering Plastics and Their Commercial Development", B. F. Foy, editor, ACS No. 96, (1969).

6. M. Matzner, L. M. Robeson, R. Barclay, Jr. and J.E. McGrath, J. Polym. Sci., Symposia, in press (1977).

7. J. E. McGrath, T. C. Ward, E. Shchori and A. J. Wnuk, Polymer Preprints, 18(1), 346 (1977).

8. J. E. McGrath, T. C. Ward, E. Shchori and A. J. Wnuk, Polymer Engineering Science, in press (1977).

9. T. A. Bush, M. E. Counts and J. P. Wightman, in Adhesion Science and Technology, Part A, L.-H. Lee, Ed., Plenum Press, New York, 1975, p. 365.

10. D. W. Dwight, M. E. Counts and J. P. Wightman, in Colloid and Interface Science, Vol. V. III, M. Kerker, Ed., Academic Press, New York, 1976, p. 143.

11. D. W. Dwight and W. M. Riggs, J. Col. and Int. Sci. 47 (3), 650 (1974).

12. D. W. Dwight in Characterization of Metal and Polymer Surfaces, Vol. 2, L.-H. Lee, Ed., Academic Press, 1977, p. 313.

13. D. T. Clark, ibid., p. 5, and references therein.

14. D. T. Clark, D. B. Adams, A. Dilks, J. Peeling and H. R. Thomas, J. Electron Spectrosc. 8, 51 (1976).

15. D. T. Clark in Advances in Polymer Friction and Wear, L.-H. Lee, Ed., Plenum Press, New York, 1975, p. 241.

16. Ginnard, C. R. and Riggs, W. M., Anal. Chem. 44, 1310 (1972).

17. O'Kane, D. F. and Rice, D. W., Polymer Preprints 16, 92 (1975).

ORIGINAL PAGE IS
OF POOR QUALITY

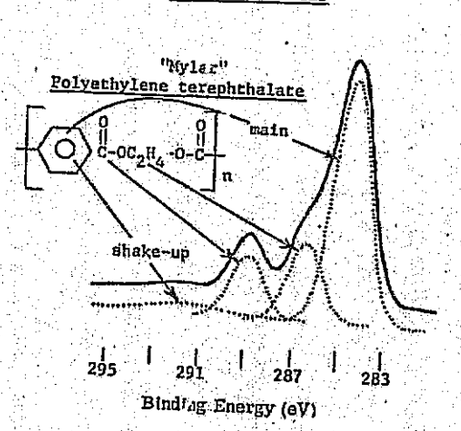

FIGURE 1

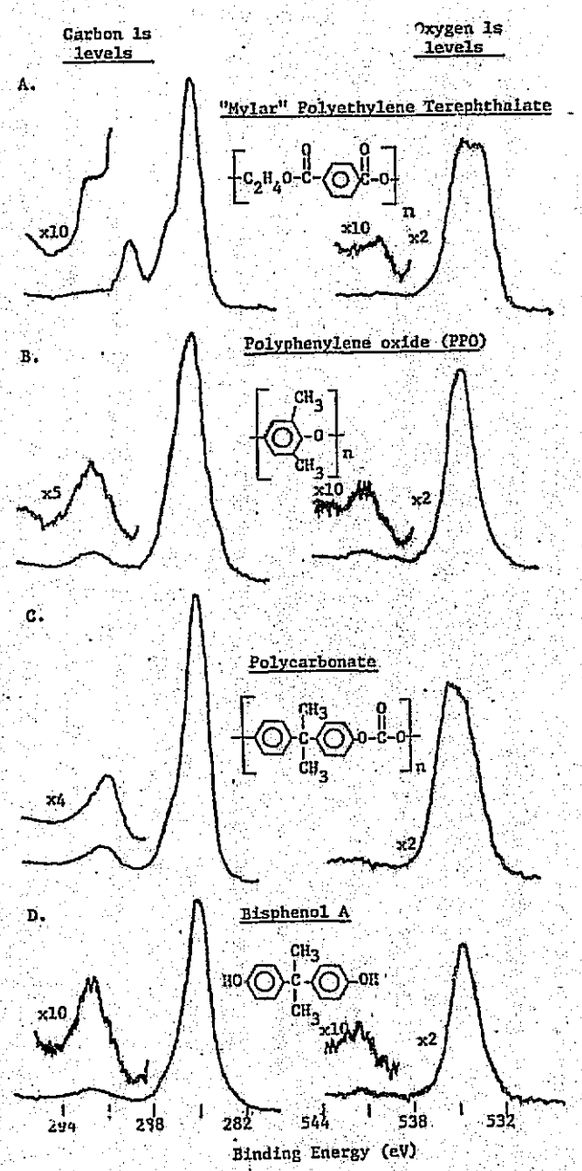

FIGURE 2

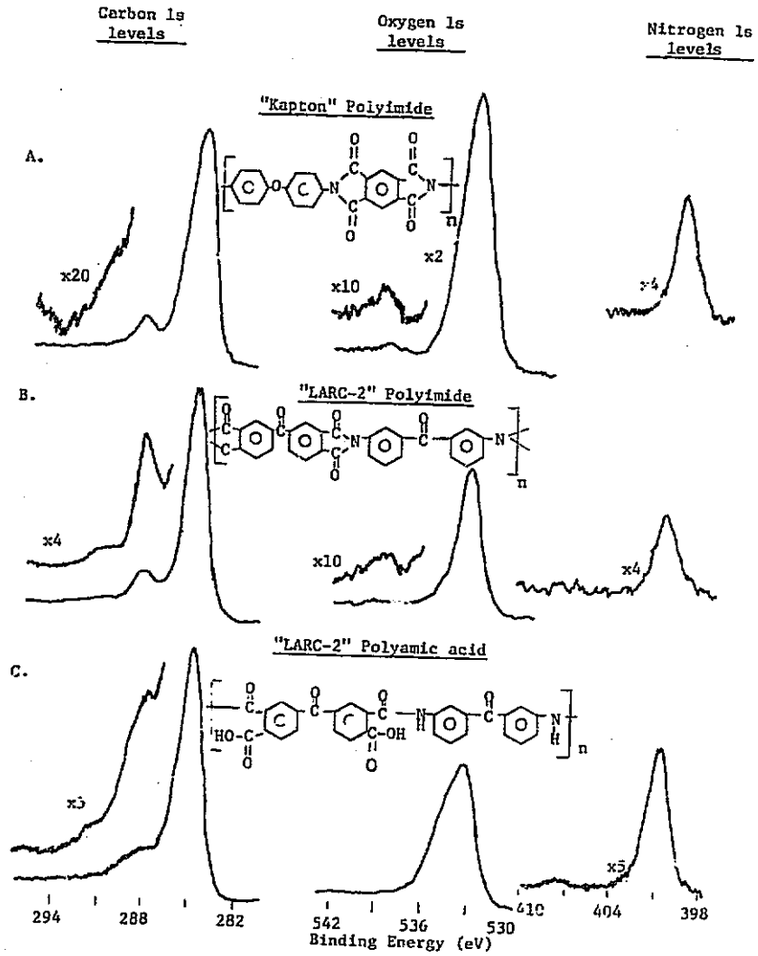

FIGURE 3

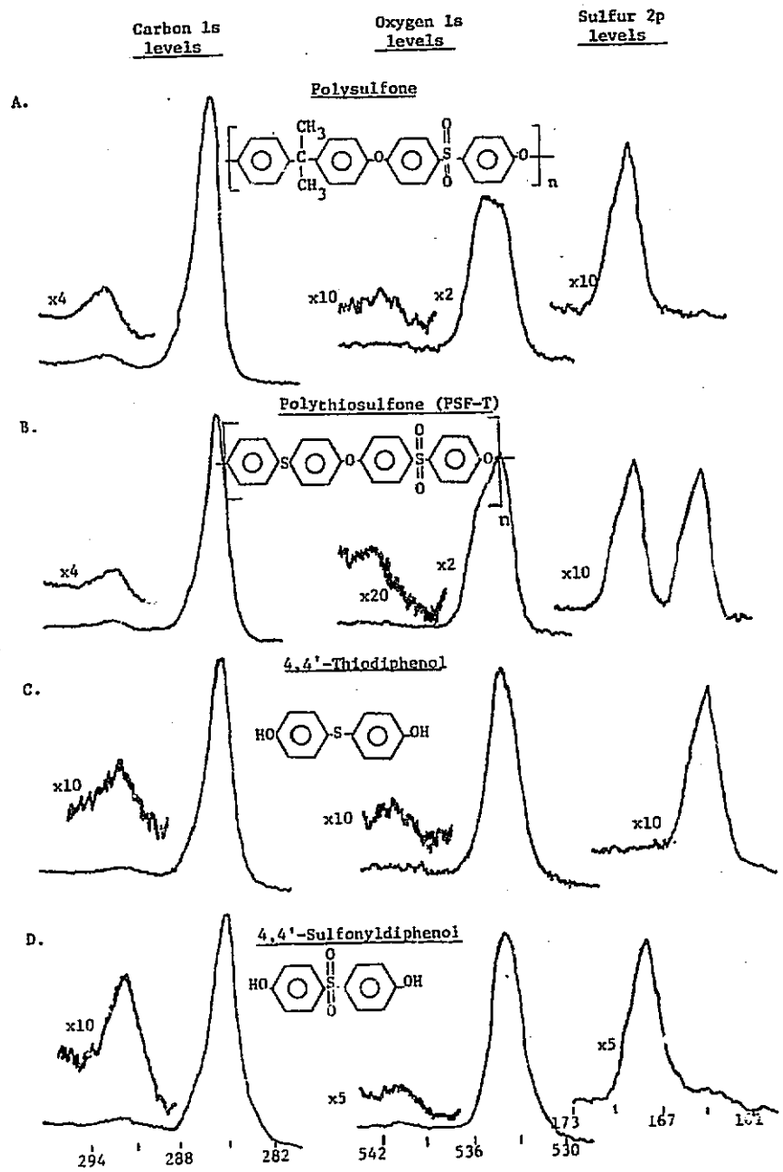

FIGURE 4

ESCA ANALYSIS OF POLYMER STRUCTURE AND BONDING. I.

David W. Dwight
Department of Materials Engineering

James E. McGrath
and
James P. Wightman
Department of Chemistry

Virginia Polytechnic Institute and State University
Blacksburg, Virginia 24061

SYNOPSIS

X-ray photoelectron spectroscopy (ESCA) provides rapid analysis of diverse polymer specimens. By determining the binding energies and intensities of core-level electrons, the atoms and functional groups in the sample surface (<10nm deep) are identified. Unsaturated systems give rise to "shake-up satellite" structures characteristic of local π-bonding. Spectra of nine engineering polymers (varying from commercial films to dilute solutions of experimental co-polymers) are presented to illustrate the potential of ESCA to identify polymer structure and bonding, and to follow chemical changes during processing.

ORIGINAL PAGE IS
OF POOR QUALITY

To be published in the Journal of Applied Polymer Science: Applied Polymer Symposia, "Polymer Analysis," J. Mitchell and T. K. Wu, Editors, Wiley Interscience, New York, 1978 (in press).

INTRODUCTION

As engineering applications for synthetic polymers continue to expand, essential research objectives include the characterization of new materials and the elucidation of relationships between structure, processing, and properties. X-ray photoelectron spectroscopy (ESCA) is a relatively new technique that provides high information content on chemical structure and bonding in thin (< 10 nm) surface layers. These unique surface-chemical parameters are of critical importance in heterogeneous systems with functional interfaces, e.g, composites and adhesives. This paper emphasizes qualitative polymer analysis, pointing out the distinctive characteristics of the ESCA method.

Siegbahn and co-workers demonstrated the general application to chemical structure analysis of kinetic energy spectroscopy of the electrons ejected from the inner shells of atoms irradiated with x-rays (1). By calculation of the characteristic binding energy of photoelectrons, the elements are identified, and the peak intensity is related to atomic concentration in the sampled volume. Furthermore, changes in the chemical environment of an atom produce "chemical shift" effects in the observed photoelectron energy; when electron density is withdrawn (oxidation), binding energy increases.

ESCA is a surface analysis technique because photoelectrons ejected from atoms deep in the sample are either self-absorbed or lose part of their kinetic energy and contribute only to spectral background. The effective escape depth varies with electron kinetic energy and sample surface structure, but can generally be estimated to be a few nanometers (2). In the decade since Siegbahn's book appeared, ESCA has elucidated a variety of problems, showing unsurpassed information content per spectrum, especially in inorganic systems (3,4), where

the different elements and oxidation states are so numerous.

During the last five years, Clark and co-workers have published a series of papers pioneering fundamental ESCA studies of polymer structure and bonding (5). Their analysis of spectra on well-characterized homogeneous polymers, model compounds, and homologous series were correlated with non-empirical, CNDO/2 SCF molecular orbital calculations. These results established that absolute and relative binding energies, and relative peak areas (intensities) are capable of elucidating many important aspects of polymer-surface chemistry. A more recent report from Clark's group has identified another level of information in the ESCA spectra of aromatic-containing polymers (6). Low-intensity, "shake-up" satellite peaks, located a few electron volts higher in binding energy than the main peak, are the result of $\pi \rightarrow \pi^*$ transitions. These data provide an additional characteristic feature for unsaturated polymers and offer the potential for new insight into π-electron distribution.

Information available from the ESCA technique, and the principal features observed in ESCA spectra are listed in Table I. Spectra represent the repeat unit in polymers because the method is an atomic spectroscopy that shows perturbation effects dependent on local molecular structure. Data collection is rapid because only a few, narrow regions of the total spectrum need to be scanned where specific atomic components are known to emit photoelectrons. There may be an advantage in simple interpretation compared to methods such as infrared and mass spectroscopy that yield a multiplicity of peaks. Another important advantage is that core-level electronic properties can be determined directly from ab initio molecular orbital calculations (5).

ORIGINAL PAGE IS
OF POOR QUALITY

TABLE I

PRINCIPAL FEATURES IN THE ESCA SPECTRA OF POLYMERS

	Spectral Feature	Information
I.	Main Peak Position	Atom identification
II.	Chemical shift	Oxidation state
III.	Peak area ratios	Stoichiometry
IV.	Shake-up satellites	$\pi \rightarrow \pi^*$ Transitions

Some polymer analysts may fear artifacts in a technique that bombards material with x-rays in a high-vacuum environment. Volatility and thermal decomposition can be minimized by cooling the sample with liquid nitrogen, but when photodecomposition is indicated, it may be necessary to extrapolate peak shape to zero exposure time (7). The effects of charging of insulating samples and contamination or other inhomogenieties in the surface layer can be difficult to take into account. However, with good standards and careful sample handling, the experimental parameters in ESCA can be adjusted to provide additional levels of information. This is especially the case when changes in surface chemistry are of most interest, e.g. weathering, and exposure to chemical or plasma etching. Details can be obtained by measuring escape depth versus take-off angle or electron energy.

In situ ion-milling experiments can provide correlative results (8). An exciting potential for future studies of multiphase polymer systems is scanning ESCA, where lateral resolution of chemical structure ($d < 20\mu m$) has been demonstrated (9).

A drop of dilute solution is sufficient to form a polymer film suitable for ESCA analysis, but special care must be taken when comparing spectra obtained from different forms, i.e. powder, fiber, film, bulk cross-section or fracture surface. Roughness may alter spectral parameters, requiring calibration. With a few spectra on known standards, ESCA can be an effective method for routine qualitative anlysis, e.g. in support of industrial quality control or synthesis research. The "fingerprint" aspect of ESCA can be effective to clarify surface effects of processing and treatments. Applications in biomedical polymers should be especially productive (10). Much more information can be elicited by detailed spectral analysis, base-line subraction, peak deconvolution, and area-ratio calculations. A heirarchy of levels of analysis and applications to polymers is outlined in Table II. A computer is very helpful for these analyses; it is a necessity for experiments in lateral or depth resolution, or to add corroborative information via molecular orbital calculations.

TABLE II

LEVELS OF ANALYSIS OF ESCA SPECTRA AND APPLICATION TO POLYMERS

I. Qualitative "Fingerprint"	A. Routine Analysis 1. Synthesis 2. Quality Control
II. Peak Area Ratios	
III. Deconvolution	B. Surface Effects 1. Treatments 2. Processing
IV. Depth Profile	
V. Molecular Orbital Calculations	C. Fundamental Correlations

Previous publication of ESCA results on polymers is dominated by fluoropolymers because of the importance of their surfaces in practical applications, and the fact that fluorine substituents cause large chemical shifts that simplify the interpretation of the carbon 1s levels (11). Fluoropolymers thus are among the best models for ESCA studies, and Clark, et al., illustrated the capabilities of ESCA to determine copolymer composition and structure, structural isomerism and the kinetics of reaction of fluorine with a poly (ethylene) surface (12). Our work in commercial "Teflon" systems revealed subtle but practically important differences in surface composition and structure, depending upon the method of forming the film (13). Combining those basic data with results after surface treatments and adhesive bond strength testing, allowed us to clarify mechanisms of adhesion and transfer (15). The mechanism of plasma polymerization and deposition of fluoropolymers also has been eludidated by ESCA (16).

Much of our earlier work with high performance thermoplastics (17-19) amd thermosets (20,21) emphasized bulk physical properties, dynamic mechanical behavior, thermal stability, durability, toughness and adhesive bond strength. Most of these engineering polymers do not contain fluorine to provide distinct chemical shifts, and overlapping peaks present a formidable problem in analysis of the ESCA spectra. Computer deconvolution illustrated below will enhance the information obtain from ESCA of polymers. However, the spectra are distinct, reproducible and unique to each of nine engineering polymers, indicating the potential of ESCA for rapid, qualitative analysis. Different qualitative features are sufficient to identify the chemical changes induced by during reactions and melt processing. In this regard, our peak shapes show good agreement with recent work demonstrating the use of ESCA to study plasma treatment of polymers (22).

ORIGINAL PAGE IS
OF POOR QUALITY

EXPERIMENTAL

Apparatus

Initial ESCA data were collected on an AEI ES-100 x-ray photoelectron spectrometer using an aluminum anode (1486.6 eV) and digital data acquisition. A Digital PDP-8e computer/plotter was used to deconvolute and display the spectra. Recently a DuPont 650 photoelectron spectrometer with a magnesium anode (1253.4 eV) and direct display of the spectra on an X-Y recorder was used. This system provide analysis of polymer samples in minutes, a significant advantage for routine work. Work is underway to apply computerized analysis of the spectra for detailed comparisons, but the qualitatively distinctive features of polymers are basically the same in both spectrometers. The lowest-energy carbon peak observed in each sample was arbitrarily assigned a value of (285.0 eV) as a means of binding energy referencing and charge correction (12). Arbitrary units of intensity are plotted on the abcissa, with scale factors relative to carbon in each sample.

Materials and Procedures

Idealized structures of the engineering polymers in this study are shown on the spectra in Figs. 1-7. The samples were obtained from the following sources. Commercial grade film of "Mylar" poly(ethylene terephathalate), pellets of nylon 6, and powder of "Tefzel" poly(ethylene/tetrafluoroethylene) were obtained from E. I. duPont de Nemours and Company. The General Electric Company supplied commercial grade pellets of "Lexan" polycarbonate and powdered poly(phenylene oxide). Commercial grade pellets of "Celcon" poly(oxymethylene) and poly(acrylonitrile) were obtained from the Celenese Corporation. Cellulose acetate was Eastman Co. "Kodacel" A22 film. An experimental polyamic acid ("LARC - 2") was supplied in 15% diglyme solution by NASA-Langley. Details

of synthesis and properties have been published elsewhere (23). Imidization of thin amic acid films was accomplished by heating in air for one hour each at 200°, 250°, then 300°C.

Several methods were employed to mount polymer samples for ESCA analysis, and we concluded that the qualitative results were not significantly affected by sample mounting. A drop or two of polymer solutions were deposited directly on the sample holder and the solvent evaporated. Coverage was determined by the absence of a signal from the metal holder. In other cases, double-sided Scotch tape circles of 0.25-in. diameter were cut with a paper punch and fastened to the holder. Polymer film samples were also punched and fastened to the tape. Powdered samples were sprinkled onto the Scotch tape and compacted with a spatula. The tape shows a silicon peak, and its absence was used to ensure complete coverage of the tape by the samples. No attempt was made to clean the samples with solvents or the like, although care was taken to avoid handling.

RESULTS AND DISCUSSION

Deconvolution of Overlapping Peaks

Many polymers show ESCA features that are combinations of two or more valence states. Assignments can be made to individual components on the basis of mathematical deconvolution illustrated in Fig. 1. Shown by the solid line are the carbon 1s levels of "Mylar" poly(ethylene terephthalate) obtained with the AEI ES-100 spectrometer. Shown in dashed lines are four Gaussian component peaks; their sum equals exactly the solid line observed experimentally. Now we can assign the main peak at 285.0 eV to the six carbons from the benzene ring, the peak at 286.8 eV to the two ester carbons and the third peak at 289.0 eV to the two carboxyl groups. At 291.5 eV a low intensity, shake-up satellite arising from the aromatic ring can be resolved. A visual approximation of the individual components will be discussed in the following examples, obtained on the DuPont 650 photoelectron spectrometer.

Qualitative "Fingerprint" Analysis

The spectra shown in Figures 2, 3, and 4 are examples of aromatic and aliphatic polymers containing carbon, oxygen and/or nitrogen. In Fig. 2 are compared poly(ethylene terephthalate) and poly(ethylene oxide), and although both are composed of aromatic and aliphatic hydrocarbon and oxygen, their spectra are clearly distinctive. In the case of poly(ethylene terephthalate), the carbon 1s region is basically identical to Fig. 1, illustrating the reproducibility of peak shape obtained from different spectrometers. Moreover, there is a good agreement with poly(ethylene terephthalate) spectra published previously (5,22). The peaks have already been assigned to aromatic, ester and carboxyl functionalities in the repeat unit. The oxygen peak is broadened

by double valence states in the carboxyl groups. Deconvolution should result in two peaks approximately one volt apart and of equal intensitity. Poly (ethylene oxide) on the other hand, has oxygen in only one environment and therefore a narrow, symmetrical peak. It is interesting to note that in both the carbon and the oxygen regions, shake-up satellites are particularly intense for this polymer. Furthermore, the main carbon peak is relatively broad due to the combination of methylene, phenyl-ether and ring carbons.

Carbon-oxygen containing polymers without aromatic rings are illustrated by spectra poly(oxymethylene) and cellulose acetate in Fig. 3. No shake-up satellites appear (the characteristic feature distinguishing aliphatic from aromatic systems). In the case of poly(oxymethylene) the carbon 1s levels show ethylene units from ethylene oxide comonomer at 285 eV and C1s acetal backbone linkages at about 288 eV. The concentration of ethylene units appears to be an order of magnitude less than the acetal linkages, consistent with the concentrations of comonomer normally employed. The carbon 1s region is complex in cellulose acetate. Distinguishable are: a shoulder at 285 eV from the alphatic groups, a main peak at 287 eV from ether linkages, and a shoulder approximately 289 eV deriving from carboxyl groups in the acetate portions. Without quantitative determination of peak-areas ratios, it is clear that the oxygen/carbon ratio in these two polymers is much greater than in the case of the other spectra shown. This is in accord with the oxygen/ carbon ratio derived from calculations based on model structures.

The introduction of a third atom, nitrogen, into polymers structures is illustrated by nylon 6 and poly(acrylonitrile) in Fig. 4. Again, the aliphatic nature of these polymers precludes the appearance of carbon shake-up satellites.

The peak for the N1s level differentiates these two polymers because of ~1 eV chemical shift between nitrile and amide nitrogens. In nylon 6 the main carbon peak derives from the aliphatic backbone units while the high energy shoulder at about 287 eV derives from the amide carbon. The carbon levels in poly(acrylonitrile) indicate the presence of carbons in two valence states and of similar quantity. Also in the poly(acrylonitrile) spectra is small oxygen peak, indicating the possibility of some surface oxidation or hydrolysis during processing.

Monomer Spectra and Comparison With Polymers

An important technique to gain confidence in peak assignments for polymers is comparison with spectra from monomers or model compounds of well-known chemical structure. Moreover, systematic studies of this kind can help to understand details of structure and bonding changes that occur during polymerization reactions.

The polycarbonate of bisphenol A is shown in juxtaposition with the monomer in Fig. 6. The differences between the C1s spectra are primarily (1) a larger feature at approximately 292 eV and (2) a shoulder around 287 eV in polycarbonate. The increased intensity in the 292 eV region for the polycarbonate derives from the carbonyl functionality added to the shake-up satellite from the aromatic rings (which also appears in bisphenol A). In the oxygen levels, the polycarbonate shows a broader peak from the two oxygen environments of the carbonyl group. The monomer, however, shows only one oxygen from the hydroxyl groups. Mathematical analysis of the spectra should show polycarbonate spectra to be the sum of bisphenol A and carbonate spectra.

The possibility of following kinetics of condensation polymerization is

shown by the ESCA spectra of a polyimide and its precursor polyamic acid in Fig. 6. The multiple environments for both carbon and oxygen in the polyamic acid broaden both carbon and oxygen levels. However, in the polyimide, the elimination of water during condensation reduces the number of valences for carbon and oxygen, and narrows the peaks correspondingly. In the carbon levels there is a main peak deriving from the armoatic rings at 285 eV and satellite structure around 291 eV. In addition, a peak about 289 eV derives from the carboxyl groups.

Effect of Processing

Most polymer processing changes the surface chemistry as illustrated in Fig. 7, which shows the carbon and oxygen levels in poly(ethylene/tetrafluoroethylene). In the original powder, two symmetrical peaks appear in the carbon region: the peak 285 eV corresponding to the hydrocarbon and the peak at 290 eV corresponding to the fluorocarbon component in the polymer. Peak-height ratio is 52 to 48, corresponding to the comonomer composition (as determined by total ignition analysis for carbon and hydrogen). Notice that there is virtually no signal in the oxygen region on the initial powder. On the other hand, after the film has been molded from the powder under heat and pressure, the spectra shown in A. are considerably different. First, a significant oxygen peak occurs, and second, the hydrocarbon peak in the carbon region has more than twice the intensity of the fluorocarbon peak. These results indicate surface oxidation during the molding step. Also, one should notice that the fluorocarbon and hydrocarbon peaks are asymmetrical on the left hand side, and are separated by 1-2 eV more than the initial powder. These ob-

servations are indications that a surface layer forms, and a charging effect is occasioned by the oxidation of hydrocarbon components at the uppermost surface.

CONCLUSIONS

Many polymer structures can be identified rapidly with the ESCA technique, and virtually any amount or form of specimen can be used. Potential applications in routine analysis where bulk and surface compositions are similar range from synthesis research to manufacturing quality control. In cases where surface composition differs from the bulk, ESCA may be the most effective way to elucidate the chemical process changes. Our conclusions are supported by results (in preparation for publication) on other polymers and copolymers, including sulfone, sulfide, siloxane, silane and quinoxaline units. It is clear that in situ depth-profile information is essential in many practical applications in order to define the extent of contamination or other in homogeneous surface layers. We are studying the effects of inert and reactive gas plasmas and ion beams for that purpose. Initial computations of polymer stoichiometry from peak heights show trends that correlate with ideal structures. A computer program is being developed to combine deconvolution with peak-area ratios, thus extracting the remaining structure and bonding information from the ESCA spectra. This background will facilitate the study of unknowns, mixtures and surface-segregation.

ACKNOWLEDGMENT

The authors would like to thank NASA and ARO for their support of this research under Grants NSG-1124 and DAAG-76-G0312, respectively.

REFERENCES

1. K. Sigbahn, C. Nordling, A. Fahlman, R. Nordberg, K. Hamrin, J. Hedman, G. Johansson, T. Bergmark, S. Karlsson, I. Lindgren and B. Lindberg, ESCA; Atomic Molecular and Solid State Structure Studies by Means of Electron Spectroscopy, Almquist and Wiksells, Uppsala, (1967).

2. P. Cadman, G. Gossedge and J. D. Scott, J. Electron Spectrosc., 13, 1, (1978).

3. D. M. Hercules, Anal. Chem., 44 (5), 106 (1972).

4. R. S. Swingle and W. M. Riggs, Crit. Rev. Anal. Chem., 267, October 1975.

5. D. T. Clark, in Characterization of Metal and Polymer Surfaces, Vol. 2, L. -H. Lee, Ed., Academic Press, (1977), p. 5.

6. D. T. Clark, D. B. Adams, A. Dilks, J. Peeling and H. R. Thomas, J. Electron Spectrosc., 8, 51 , (1976).

7. R. Phillips, J. Colloid and Interface Sci., 7 (3), 687 (1974).

8. D. E. Williams and L. E. Davis in Characterization of Metal and Polymer Surfaces, Vol. 2, L. -H. Lee, Ed., Academic Press, (1977), p. 53.

9. C. T. Hovland, Appl. Phys. Let., 30 (6), 274 (1977).

10. J. D. Andrade, G. K. Iwamoto and B. McNeil, in Characterization of Metal and Polymer Surfaces, Vol. 2, L. -H. Lee, Ed., Academic Press, (1977), p. 113.

11. C. R. Ginnard and W. M. Riggs., Anal. Chem., 44, 1310 (1972).

12. D. T. Clark, in Advances in Polymer Friction and Wear, L. -H. Lee, Ed., Plenum Press, New York, New York, (1975), p. 241.

13. D. W. Dwight, in Characterization of Metal and Polymer Surfaces, Vol. 2, L. -H. Lee, Ed., Academic Press, (1977), p. 313.

14. D. W. Dwight and W. M. Riggs, J. Colloid and Interface Sci., 47, (3) 650 (1974).

15. D. W. Dwight, J. Colloid and Interface Sci., 59 (3), 447 (1977).

16. D. F. O'Kane, and D. W. Rice, Polymer Preprints, 16, 92 (1975).

17. A. Noshay and J. E. McGrath, Block Copolymers: Overview and Critical Survey, Academic Press, New York, (1977).

ORIGINAL PAGE IS
OF POOR QUALITY

18. J. E. McGrath, T. C. Ward, E. Shchori and A. J. Wnuk, Polymer Engineering Science, 17 (8), 647 (1977).

19. J. E. McGrath, T. C. Ward, E. Shchori, A. J. Wnuk, R. Viswanathan, J. S. Riffle and T. F. Davidson, Polymer Preprints, 19 (1), 109 (1978).

20. T. A. Bush, M. E. Counts and J. P. Wightman, in Adhesion Science and Technology Part A, L. -H. Lee, Ed., Plenum Press, New York, (1975), p. 365.

21. D. W. Dwight, M. E. Counts and J. P. Wightman, in Colloid and Interface Science, Vol. V. III, M. Kerker, Ed., Academic Press, New York, (1976) p. 143.

22. H. Yasuda, H. C. Marsh, S. Brandt and C. M. Reilley, J. Polymer Sci. (Chem,)15, 991, (1977).

23. T. L. St.Clair and D. J. Progar, in Adhesion Science and Technology, Part A, L. -H. Lee, Ed., Plenum Press, New York, (1975), p. 187.

FIGURE CAPTIONS

FIGURE 1 Carbon 1s ESCA spectrum from poly(ethylene terephthalate)"Mylar" film. Experimental peak shape is shown by the solid line. After deconvolution into four Gaussian components (dashed lines) the assignments to the structural features indicated was straight forward. The 6:2:2 ratio of carbon functionality is reflected approximately by the component peak areas.

FIGURE 2 Complete ESCA spectra from A. poly(ethylene terephthalate) showing functionality of three types for carbon and two types of oxygen. B. poly(phenylene/oxide) showing a single oxygen type, broadening of the carbon main peak and relatively strong shake-up satellites.

FIGURE 3 ESCA spectra of poly(oxymethylene) and cellulose acetate. These aliphatic polymers show no shake-up satellites. In poly(oxmethylene), the low-energy carbon peak indicates a relatively small concentration of ethylene linkages in the backbone. In cellulose acetate a broad C1s peak involves (1) a shoulder at 285 eV (2) a main peak at 287 eV and (3) a shoulder at 289 eV. In both polymers, the oxygen to carbon ratio is considerably greater than the other examples (a trend expected from the structures).

FIGURE 4 ESCA spectra of nylon 6 and poly(acrylonitrile). These examples include a third element, nitrogen, and poly(acrylonitrile) appears about 1 eV lower in binding energy than the nitrogen in the backbone of nylon 6. The carbon spectra will yield more information after deconvolution, but is qualitatively clear that there are two or possibly three electronic environments for carbon in both polymers. There is an oxygen peak in poly(acrylonitrile) indicating surface oxidation or hydrolysis during processing.

FIGURE 5 ESCA spectra of polycarbonate and its monomer, bisphenol A., illustrating a common procedure in basic data collection for ESCA spectroscopy. Since the results from polymers derive from the average of repeat units, spectra of monomers can be used to confirm polymer assignments. The spectral features of polycarbonate that differ from bisphenol A can be attributed to the carbonate group in the polymer. This group creates a peak in the same region as the shake-up satellite in carbon as well as a shoulder on the left hand side of the main carbon peak. Also, the two environments for oxygen broaden the oxygen peak.

FIGURE 6 ESCA spectra from an experimental polyamic acid and polyimide. This pair spectra illustrate the potential for ESCA to follow curing reactions. The multiple carbon and oxygen environments in the polyamic acid broaden the carbon and oxygen levels. After heat cure and elimination of water, the polyimide shows considerably sharpened peaks in carbon and oxygen levels.

FIGURE 7 ESCA spectra of the carbon and oxygen levels in "Tefzel" poly(ethylene/tetrafluoroethylene) (A.) after molding into a film, and (B.) original powder. The spectra illustrate surface effects occasioned by processing. (A.) shows a significant oxygen peak. The carbon peaks broaden asymmetrically on the left hand side and the hydrocarbon peak appears twice as intense as the fluorocarbon peak. Oxidation of the surface during molding is indicated.

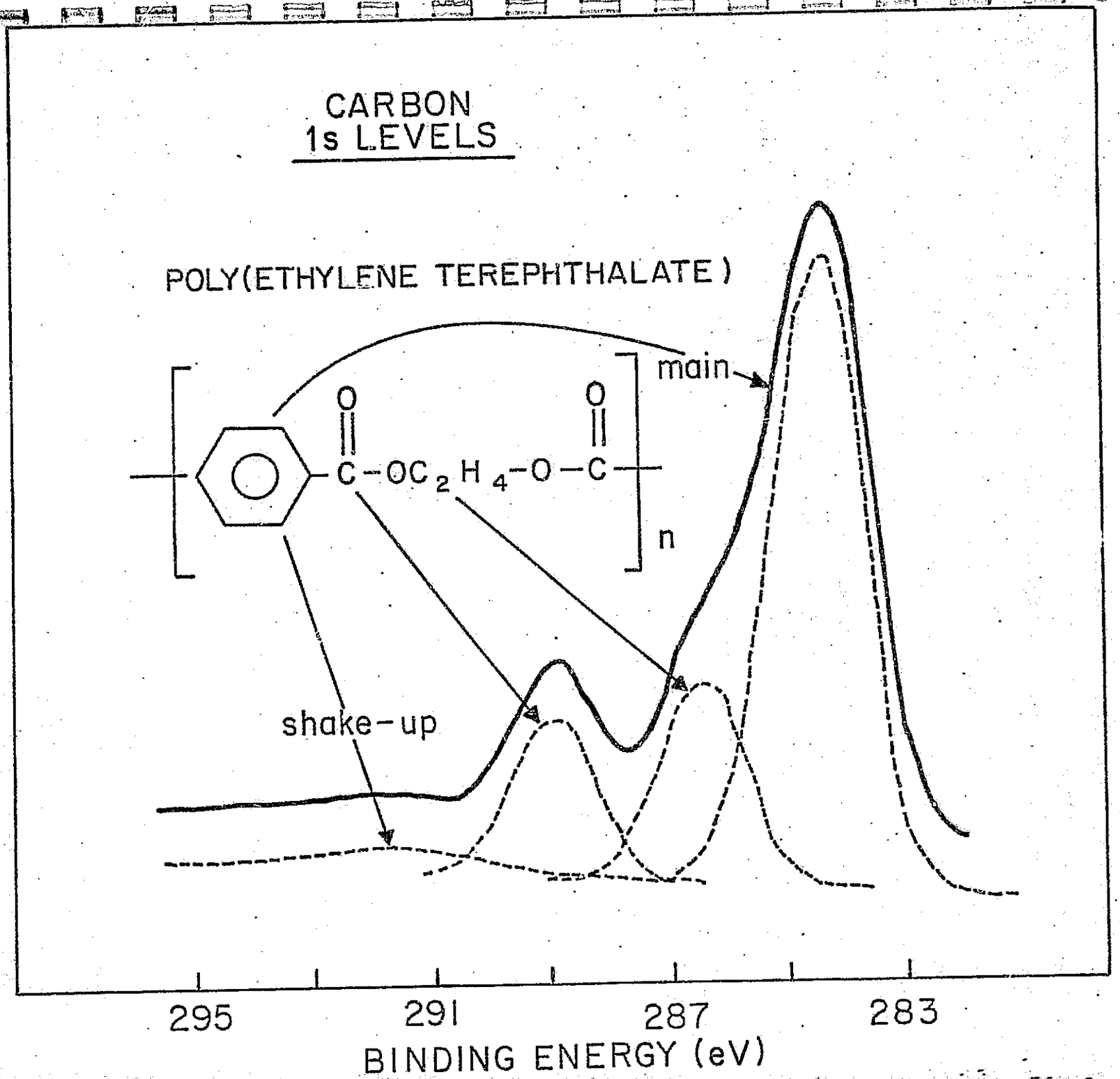

ORIGINAL PAGE IS
OF POOR QUALITY

Fig. 1

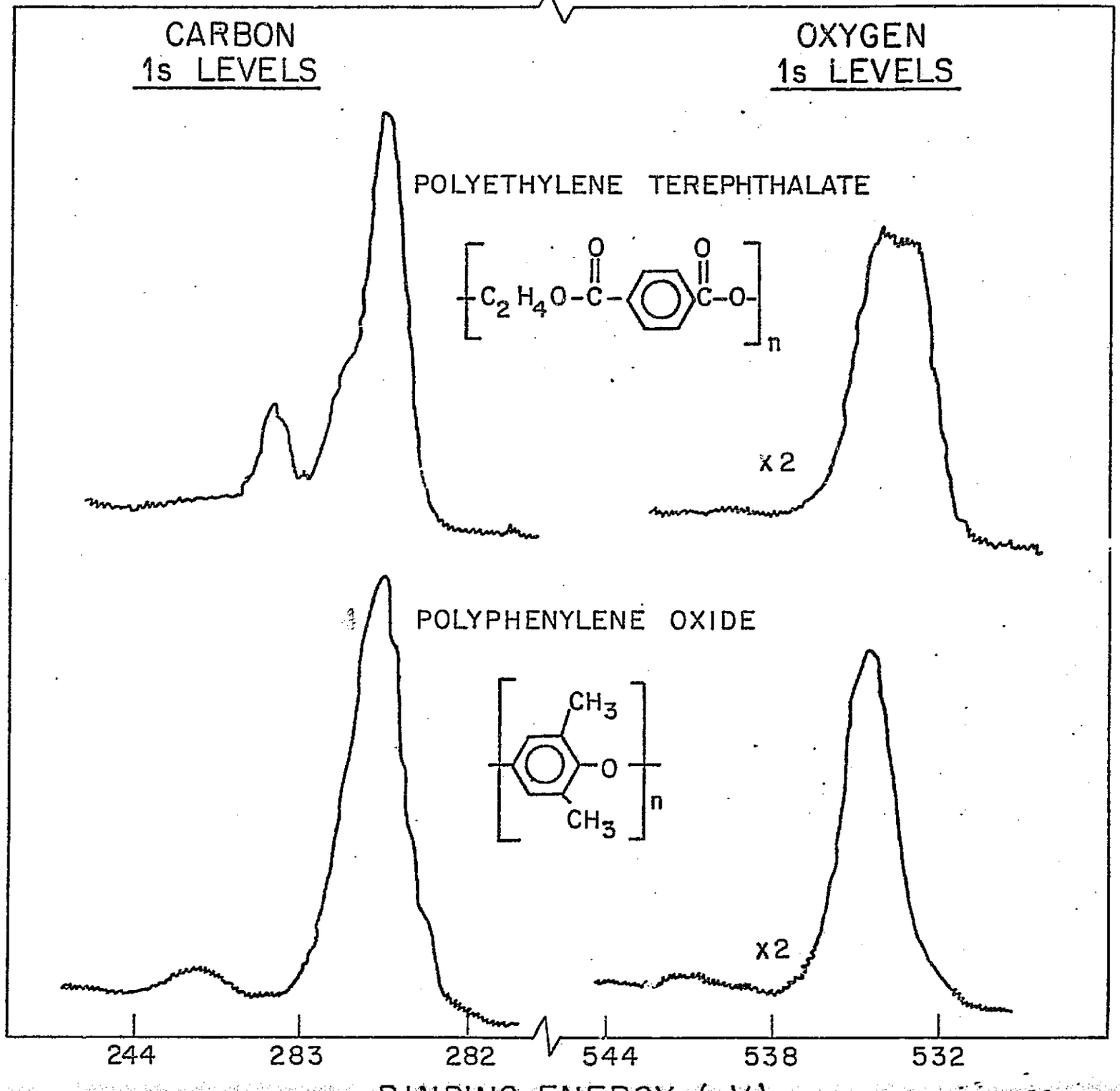
CARBON
1s LEVELS
OXYGEN
1s LEVELS
POLYETHYLENE TEREPHTHALATE
$-[C_2H_4O-C(=O)-C_6H_4-C(=O)-O-]_n$
x2
POLYPHENYLENE OXIDE
$-[C_6H_3(CH_3)-O-C_6H_3(CH_3)]_n$
x2
244
283
282
544
538
532
BINDING ENERGY (eV)

Fig. 2

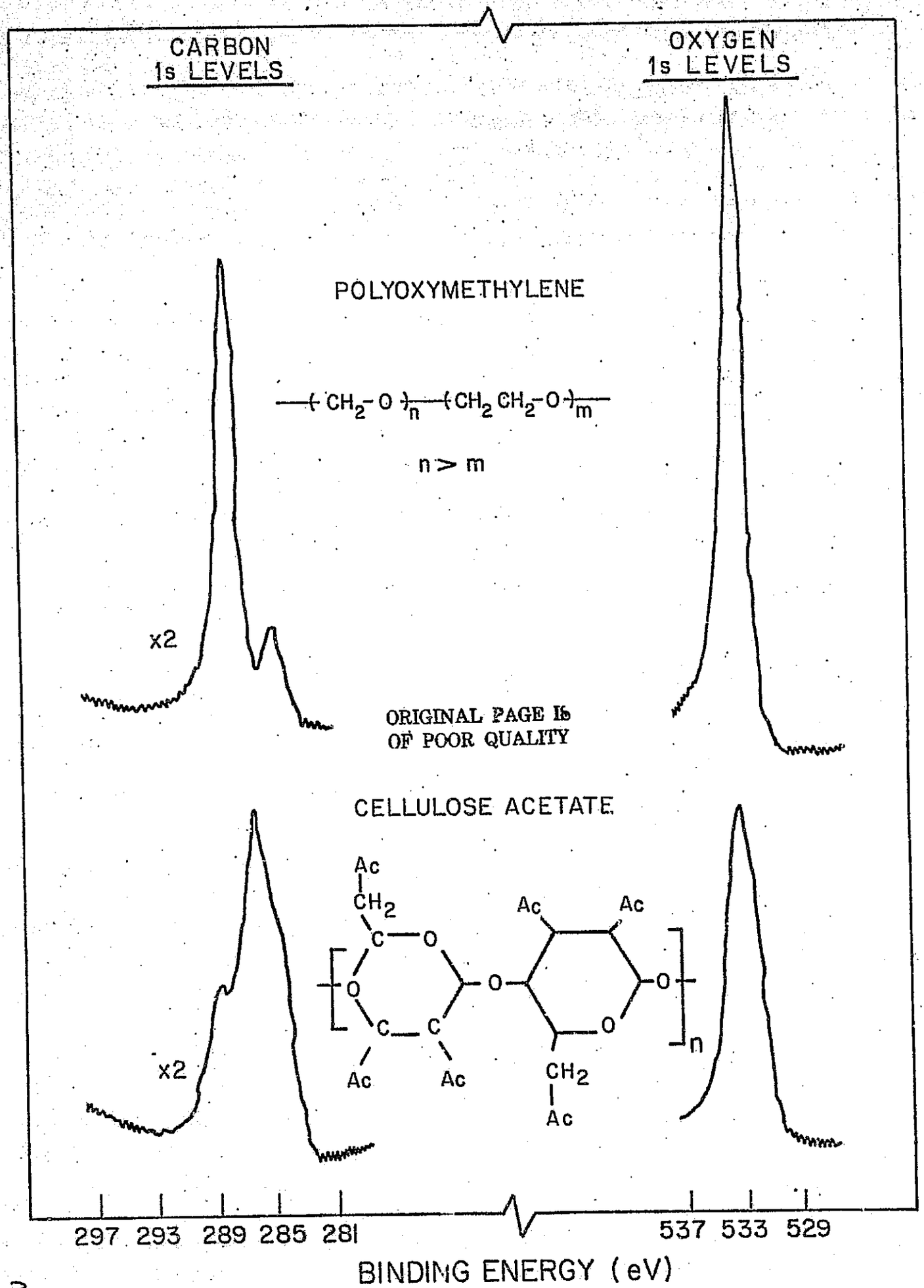
CARBON
1s LEVELS
OXYGEN
1s LEVELS
POLYOXYMETHYLENE
n > m
x2
ORIGINAL PAGE IS
OF POOR QUALITY
CELLULOSE ACETATE
x2
297 293 289 285 281
537 533 529
BINDING ENERGY (eV)

Fig.3

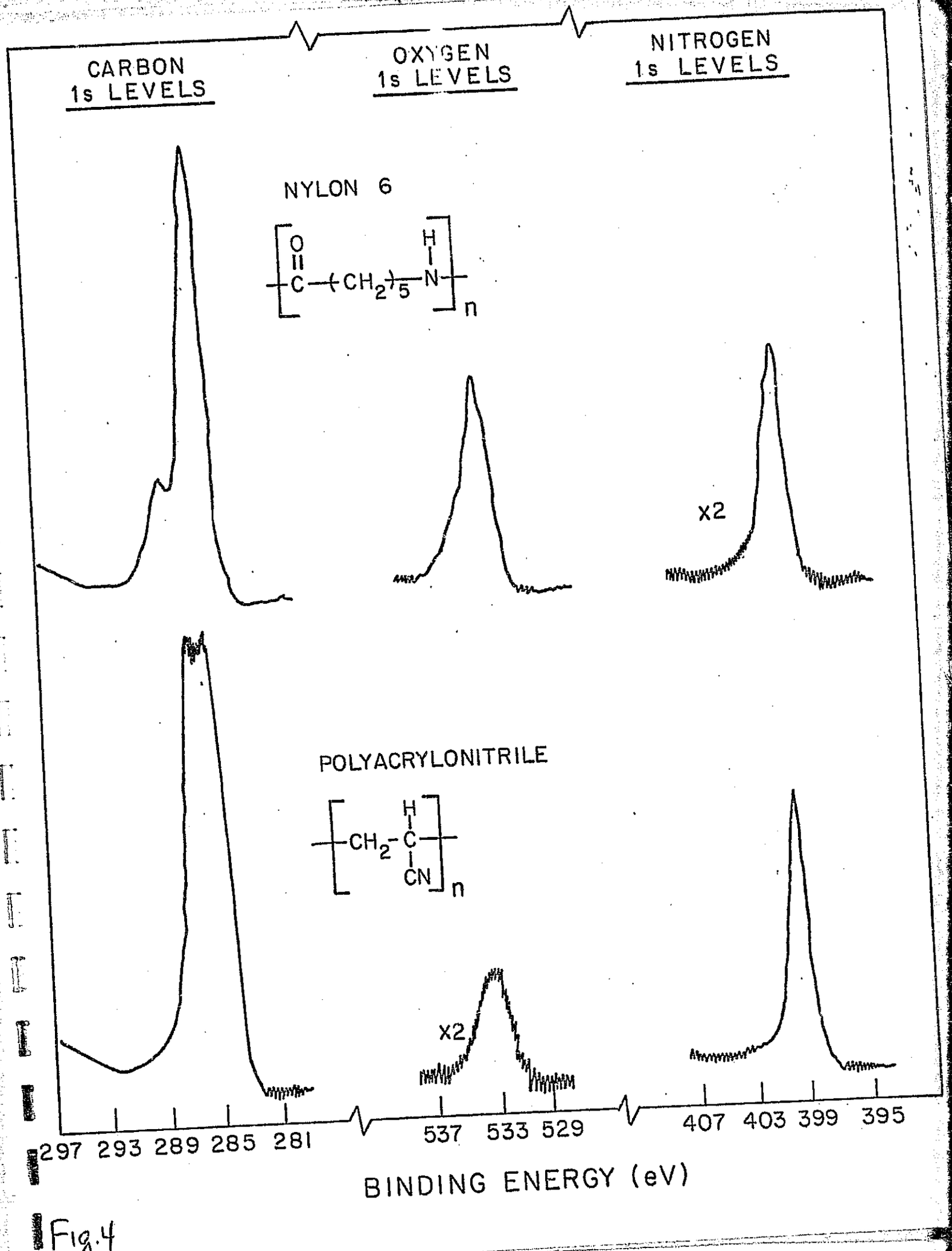
CARBON
1s LEVELS
OXYGEN
1s LEVELS
NITROGEN
1s LEVELS
NYLON 6
x2
POLYACRYLONITRILE
x2
297 293 289 285 281
537 533 529
407 403 399 395
BINDING ENERGY (eV)

Fig. 4

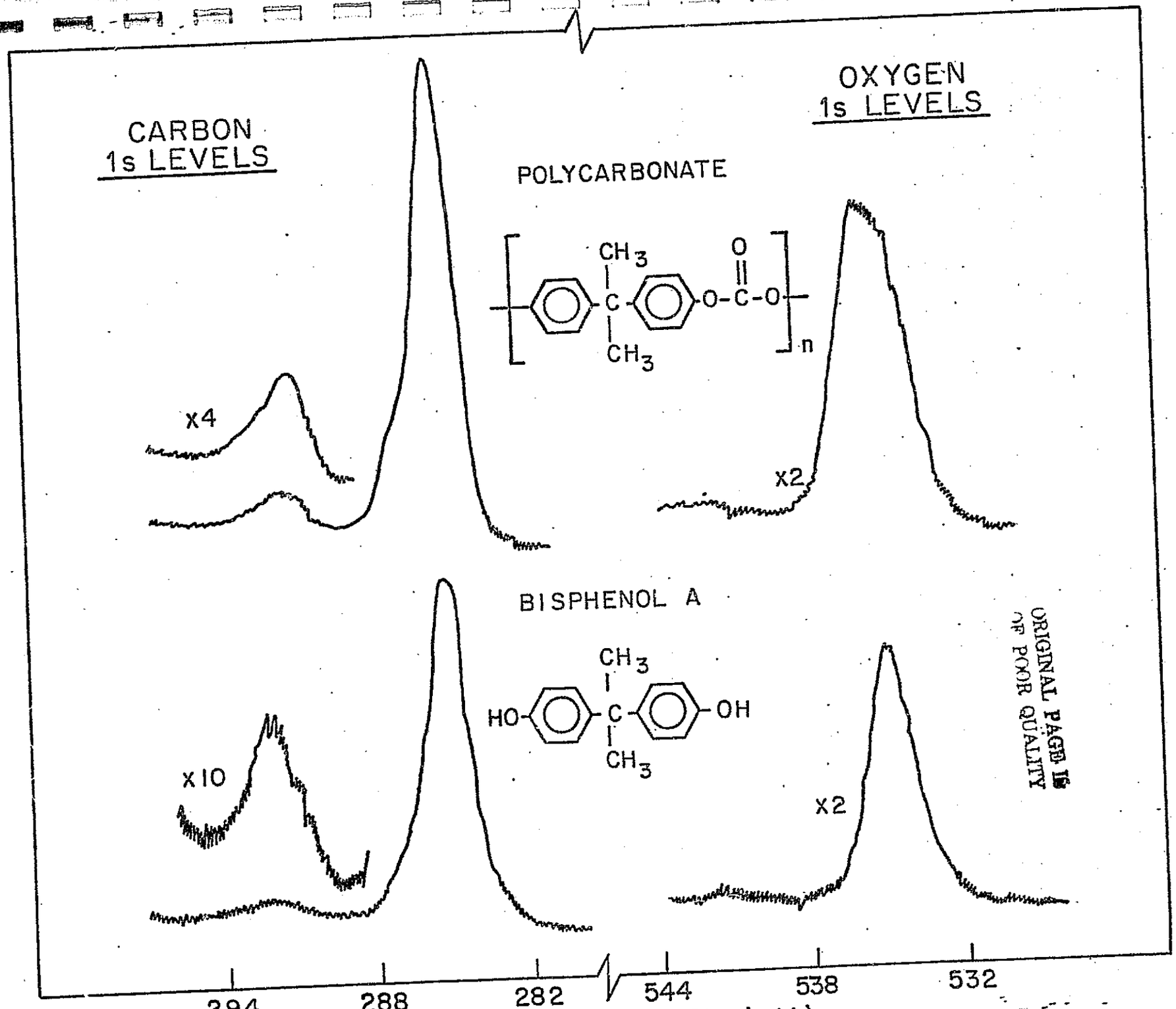

ORIGINAL PAGE IS
OF POOR QUALITY

Fig. 5

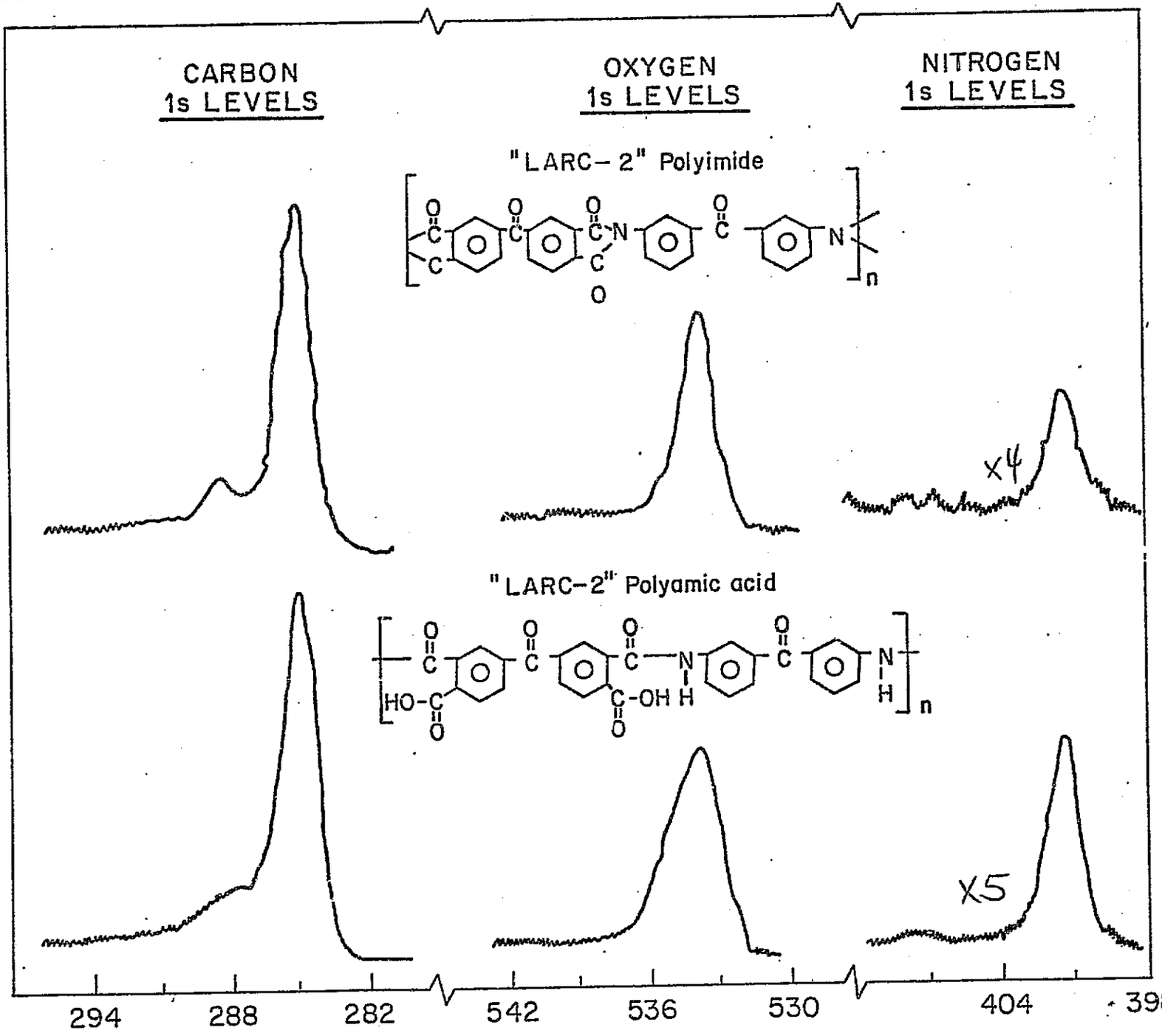
CARBON
1s LEVELS
OXYGEN
1s LEVELS
NITROGEN
1s LEVELS
"LARC-2" Polyimide
x4
"LARC-2" Polyamic acid
x5
294
288
282
542
536
530
404
398
BINDING ENERGY (eV)

Fig 6

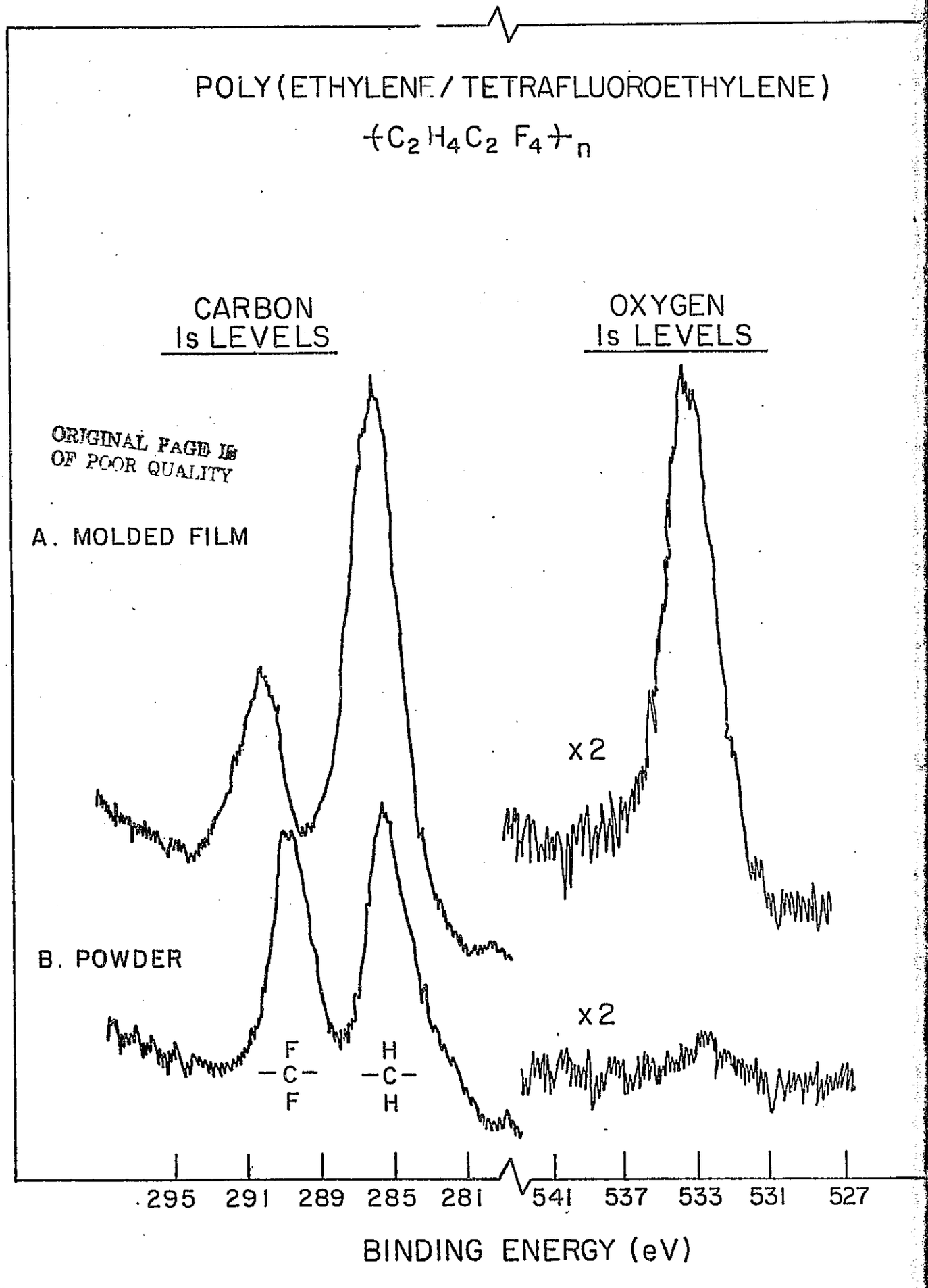
POLY(ETHYLENE/TETRAFLUOROETHYLENE)
$+C_2H_4C_2F_4+_n$
CARBON
Is LEVELS
OXYGEN
Is LEVELS
ORIGINAL PAGE IS
OF POOR QUALITY
A. MOLDED FILM
B. POWDER
x2
x2
F
—C—
F
H
—C—
H
295
291
289
285
281
541
537
533
531
527
BINDING ENERGY (eV)

Fig. 7